SCK • CEN
STUDIECENTRUM VOOR KERNENERGIE
CENTRE D'ÉTUDE DE L'ÉNERGIE NUCLÉAIRE

SCIENTIFIC REPORT
SCK•CEN-BLG-950

A First Step Towards a Multiscale Modelling of Fe-Cr Alloys

Validation and discussion of existing empirical interatomic potentials for Fe-Cr alloys

Pär Olsson*, Lorenzo Malerba and Abderrahim Almazouzi

* Department of Neutron Research, Ångström Laboratory, Uppsala University (Sweden)

June, 2003

SCK•CEN
Boeretang 200
2400 Mol
Belgium

UT-MOD Fusion Task

SCIENTIFIC REPORT OF THE BELGIAN NUCLEAR RESEARCH CENTRE
SCK•CEN-BLG-950

A First Step Towards a Multiscale Modelling of Fe-Cr Alloys

Validation and discussion of existing empirical interatomic potentials for Fe-Cr alloys

Pär Olsson*, Lorenzo Malerba and Abderrahim Almazouzi

* Department of Neutron Research, Ångström Laboratory, Uppsala University (Sweden)

June, 2003
Status: Unclassified
ISSN 1379-2407

SCK•CEN
Boeretang 200
2400 Mol
Belgium

UT-MOD Fusion Task

© SCK•CEN
Belgian Nuclear Research Centre
Boeretang 200
2400 Mol
Belgium

Phone +32 14 33 21 11
Fax +32 14 31 50 21

http://www.sckcen.be

Contact:
Knowledge Centre
library@sckcen.be

Abstract

High chromium ferritic/martensitic steels are candidate structural materials for future fusion reactors and Accelerator Driven Systems (ADS). Their use for these applications requires a careful assessment of their mechanical stability under high energy neutron irradiation and in aggressive environments. In particular, the Cr concentration has been shown to be a key parameter to be optimised in order to guarantee the best corrosion and swelling resistance, together with the least embrittlement. Although experimental studies seem to suggest 9% Cr to be the optimal concentration, no clear physical understanding supports this choice. The multiscale modelling approach can in this framework provide insightful information about the mechanisms playing a role in determining the response to irradiation of Fe-Cr alloys. The starting point for such an approach is the development and validation of an adequate Fe-Cr interatomic potential, ready for use in atomistic simulations.
Recently, four Embedded Atom Method (EAM) potentials for the description of different Fe-Cr alloys have been fitted in by the KTH/U.Uppsala Swedish group, in the framework of SPIRE, an ADS-oriented 5th Framework Programme shared-cost project of the European Commission. Here these potentials are used to calculate, using Molecular Statics (MS) and Dynamics (MD) techniques, a series of magnitudes of importance for the description of point defect formation and migration and their interaction with solute atoms. The values found with the different potentials are compared between them and, when available, with results from other existing interatomic potentials, *ab initio* calculations and experimental data. Strong and weak points of these potentials are thereby defined and discussed. The concept of *concentration-dependent* potential is also discussed. Finally, Atomistic Kinetic Monte Carlo (AKMC) simulations have been performed using these potentials to assess their capabilities of reproducing the behaviour of Fe-Cr alloys in selected conditions.
The work shows that, within the known limits of the EAM approach, a potential of use for a first assessment of primary damage state after displacement cascades in Fe-Cr alloys, in the region around 10% Cr, is now available.

The work reported here is the first result of the collaborative effort started recently between SCK•CEN and the University of Uppsala, together with the Royal Institute of Technology of Stockholm (KTH), towards a multiscale modelling of Fe-Cr alloys, opened with the short stay of P. Olsson at SCK•CEN, supported by the mobility fund scheme of the European fusion programme (Agreement for the Promotion of Staff Mobility No. 131-83-7 FUSC), in the framework of the Fusion Underlying Technology task.

Table of contents

1 Introduction

High-chromium (9-12wt%) ferritic/martensitic steels have been considered since the late 1970s as potential first-wall and breeding-blanket structural materials in future fusion reactor systems [1]. More recently, they have also been considered as candidate structural materials for accelerator-driven systems (ADS) [2]. Both in a fusion reactor and in an ADS, the structural materials are expected to be exposed to particularly harsh neutron irradiation and environment, far harsher than in current LWR (light water reactor) nuclear plants. Neutron irradiation is well known to induce a degradation of the mechanical properties of the materials, which is drastically enhanced if, in addition, nuclear transmutation (H and He production) takes place, as is expected with high energy neutrons. These effects are detrimental to the structural function itself and may cause safety problems during routine operation. Activation from nuclear transmutation will also cause problems for decommissioning and waste disposal. Therefore, any structural material for the above-mentioned nuclear applications should be able to preserve as much as possible its mechanical and thermal properties after prolonged irradiation, while becoming activated as little as possible. The chemical composition of high-Cr steels can be tuned so as to minimise the level of activation after neutron irradiation (so called *reduced-activation ferritic-martensitic* - RAFM - steels), without significant loss of mechanical performance, as compared to conventional steels. In addition, their behaviour under irradiation is expected to be better than, for example, austenitic steels, which are severely penalised not only by high swelling, but also low thermal conductivity [3]. However, the degradation of mechanical properties due to prolonged high energy neutron irradiation remains the most critical issue to be investigated and mastered in view of the use of these steels for fusion or ADS applications.

High-Cr ferritic steels have been used as cladding material in fast breeder reactors and many experimental data about their behaviour under irradiation come from the research effort to optimise this type of steels for this application. Swelling is known to be the decisive factor limiting the performance of these steels in a fast breeder reactor, thereby limiting also fuel burnup. The discovery of swelling was made in 1967 in the Dounray Fast Reactor [4] and since then a large experimental effort has been devoted to finding steel compositions that are more resistant to irradiation-induced swelling. The incubation threshold for the onset of accelerated swelling has been found to be much higher in high-Cr ferritic-martensitic steels (like the conventional T91) than in austenitic steels [5].

One additional difficulty inherent to the choice of structural materials for fusion applications (and, to a lesser extent, also ADS) is that up to the present day no available neutron source is capable of reproducing the hard neutron

spectra expected in reactors of this type. Therefore, any prediction about the behaviour of materials used in such systems must be extrapolated from data obtained by irradiating using available facilities. In order to be able to rely on such extrapolations, it is paramount not only to gather new experimental data, pushing the materials towards more realistic irradiation conditions, but also to achieve a satisfactory understanding of the physical mechanisms of property degradation, from the microscopic to the macroscopic level.

Until less than a decade ago the candidate materials for structural use in future fusion reactors were, particularly in Europe, mostly 12%-Cr steels [6]. These steels were chosen for their supposed high swelling and corrosion resistance. However, several investigations showed that too high Cr content may lead to unacceptable embrittlement under irradiation [7], which has been recently correlated to α' phase precipitation [8]. For this reason, the composition of the steels proposed for fusion applications has progressively shifted towards lower Cr contents: either 7%, as in the Japanese F82H steel, or 9% Cr, as in the Eurofer. On the basis of a series of interesting experimental observations, the latter appears to perform better than the others [6,9,10]. However, there is still a serious lack of experimental data, that prevents any conclusion from being definitively drawn. Moreover, the ultimate physical reasons why this shift in composition is actually beneficial are completely unknown and complex temperature effects have been observed [7]. This gap in the comprehension of the physical mechanisms underlying the behaviour of these steels should be overcome: it is indeed desirable that a robust choice of the steel composition rely on the understanding of the physical mechanisms behind the performance of the material. Hence the importance of rationalising experimental data using a modelling approach capable of identifying the fundamental physical mechanisms governing production and evolution of radiation damage. The multiscale modelling approach is a promising one for this purpose.

The theoretical understanding of the mechanisms responsible for swelling of neutron irradiated steels remains on a qualitative level. The production bias model (PBM), originally suggested by Woo and Singh, has been able to reproduce swelling rates for fcc-copper irradiated up to 1 dpa [11–13]. In this model, it is assumed that the main driving force for swelling is the aggregation of interstitial clusters during the recoil cascade, and their subsequent one-dimensional migration to grain boundaries and other sinks. Vacancies will tend to form immobile clusters and remain in the bulk. The effective transport of atoms from the bulk to the surface brought about by this mechanism gives rise to void swelling. Nevertheless, the well known difference in swelling rates between face centered cubic (fcc) and body centered cubic (bcc) crystals [14] remains unexplained within the PBM framework. A number of molecular dynamics (MD) simulations of displacement cascades with interstitial cluster formation have been performed for pure bcc-iron and fcc-copper [15–17]. Even though these simulations indicate that there is a difference in cluster size and

formation rate between these two metals [17], this primary damage difference is probably not enough to explain the experimental findings [14].

The reliability of atomistic simulations depends strongly on the validity of the effective interaction potential adopted to describe interatomic forces and calculate the total energy of the system. Historically, the first many-body potentials applicable to large systems were developed in the 1980s using the Embedded Atom Method (EAM) [18] or the Finnis-Sinclair (FS) [19] approach, fitted on experimentally measured properties of the concerned metals. For example, a short-ranged potential of Finnis-Sinclair type, further developed at Liverpool University, has been widely used to simulate displacement cascades in bcc-Fe [15,16]. This potential is able to describe the initial hot phase of the recoil cascade and has been extensively used also to study the defect configurations that characterise the primary damage state [20]. Likewise, a long range EAM potential for bcc-Fe was developed by Simonelli and co-workers [21] and also used for displacement cascade simulations [22]. For these simulations, it is customary to merge the potentials, which are generally fitted to equilibrium or quasi-equilibrium configurations, to a high-energy repulsive potential, generally chosen to be of Ziegler-Biersack-Littmark (universal potential) type [23]. The way the connection between repulsive and attractive part is done is known to influence in a significant manner the type of primary damage state predicted by the potential and the criterion typically used to adjust the connecting function, which is often of Born-Mayer type [15], is a fitting to experimentally determined threshold displacement energies for the metal of concern. However, it has been shown that even this condition is not enough to guarantee homogeneous results [22]. More generally, different interatomic potentials may predict different alloy behaviours as far as, for example, the interaction between point-defects and solute atoms is concerned, as is being witnessed more and more in the case of Fe-Cu alloys [24]. Thus, it appears important to improve the quality of existing potentials for their use in atomistic simulations of iron and iron alloys, and equally important to conduct a careful evaluation of the performance of the fitted potentials in predicting key magnitudes for radiation damage simulations, in comparison with available experimental results and predictions from other methods, such as *ab initio* calculations, as well as other potentials, in order to be aware of the limits of the potential in use.

On the other hand, discrepancies exist also on the experimental side regarding e.g. the behaviour of pure iron subject to neutron irradiation cascades. This is illustrated for example by the fact that the measured swelling rate in pure Fe varies from 0.03% per dpa up to 0.5% per dpa at the same temperature [25,26].
For Fe-Cr alloys less data are available from experiments than for Fe but they seem to give a more or less consistent picture. Irradiation campaigns on Fe-Cr alloys with varying fractions of Cr have been conducted in the reactors EBR-II,

FFTF and DFR [5], with the following results: At doses below 15 dpa(where the impact of He generation can be neglected), the data exhibit minimum swelling rates for Cr concentrations ranging from 2 to 6 percent; a maximum is observed for 9-12% Cr, with decreasing rate of swelling for concentrations of Cr greater than 12%. It has been also observed that the addition of even small percentages (0.1%) of Cr to ultra-pure Fe induces more frequent nucleation of small loops of interstitial nature, as compared to ultra-pure Fe, since the early stage of the irradiation, as well as faster loop growth, both using neutrons and electrons, in a range of irradiation temperatures between 200°C and 500°C [27]. An enhancement of the loop density in electron irradiated Fe-10%Cr at 25°C, as compared to pure Fe, has been found as well by Yoshida *et al.* [28]. These experimental findings point towards some kind of interaction between Cr atoms and self-interstitial atoms in Fe-Cr alloys. Indeed, the formation of stable mixed Fe-Cr dumbbells has been experimentally deduced by Maury and co-workers [29]. The complex swelling -behaviour can hence probably be rationalised, in a PBM framework, by assuming a complex influence of Cr on self-interstitial atoms (SIA) and SIA-cluster mobility, as well as void formation. Atomistic investigations of the interaction between Cr atoms and point defects will hence help cast some light on the problem.
Another characterising phenomenon observed in Fe-Cr alloys is the precipitation (or nanosegregation) of α' phase, which seems to correlate well with the dependence of steel embrittlement on Cr concentration, independently of the concentration of other solute atoms [8]. Under irradiation, at operation relevant temperatures, this segregation seems to be faster than under simple thermal ageing [8] and to take place even for Cr concentrations below the miscibility gap predicted by currently available phase diagrams [30]. In this context, too, atomistic studies could give a substantial contribution to the understanding of the segregation phenomenon.

For all these purposes, an interatomic potential to describe Fe-Cr alloys is needed. This interatomic potential, implemented in atomistic simulation codes, should prove able to describe, as correctly as possible, the expected interaction with self-interstitial atoms, as well as the formation of α' phase in experimentally proved conditions (see e.g. [31,30]). The objective of this work is to produce a critical assessment of a series of recently fitted EAM potentials for Fe-Cr alloys, in view of their improvement and use for displacement cascade MD simulations and, more generally, radiation damage studies conducted using atomistic simulation techniques.

We start by shortly describing the general framework of the multiscale modelling of radiation damage and the theories behind each of the main modelling modules. *Ab initio* results and the type of interatomic potentials used in this work will also be briefly outlined as a prerequisite. The reported work will consist mainly of the validation of the Fe-Cr interatomic potentials, by comparison with *ab initio* and, to a lesser extent, experimental values, for magnitudes of

interest for radiation damage description (defect formation energies, binding energies and migration energies mostly). In addition, the trends predicted by the potentials will be checked also for magnitudes not known from *ab initio* calculations or experiments, but useful to evaluate what we should expect to get from them, when applied to radiation damage studies. Finally, the potentials will be used for atomistic kinetic Monte Carlo (AKMC) simulations, in order to assess their capability to predict Cr-rich phase precipitation. The meaning and relevance of the results of the presented calculations will be discussed.

2 Multiscale Modelling

To come to as good an understanding as possible of complex physical phenomena it is often necessary to work through several overlapping theories and models of description. This is particularly true when studying radiation damage in materials. Neutron damage production and evolution are inherently multiscale and multiphysics phenomena. The process starts with the interaction of neutrons with matter, which occurs on timescales shorter than femtoseconds and involves nuclear reactions and neutron transport phenomena, studied respectively in nuclear physics and neutronics. The main outcome of the impingement of neutrons on matter is the creation of displacement cascades: sequences of atomic displacements that, within a few picoseconds at the most, leave a local supersaturation of point defects (vacancies and interstitials) in a very small region of material. The displacement cascades are complex phenomena that cannot be observed experimentally, but can be studied for example using molecular dynamics, based on the assumption that Newtonian mechanics and a many-body empirical interatomic potential are enough to describe the multiple events that characterise them. The distribution of point defects and point defect clusters left by the cascade is referred to as *primary damage state* and its features may greatly vary from material to material [17]. These defects can then migrate, according to diffusion laws, towards defect sinks (dislocations, grain boundaries) or act as nuclei for the formation of complex secondary defects. The evolution of defect features in irradiated materials is a continuous process that covers timescales as long as the exposure to irradiation itself. In nuclear reactors, this can go on for years. Eventually, the interaction between irradiation-induced and pre-existing defects, particularly dislocations and grain boundaries, in interplay with the chemical composition and, in some cases, new elements created by transmutation (H, He) determines radical changes in the macroscopic properties of the material. The effects of these property changes on the performance of the material can be certainly evaluated with classical mechanical tests, but their causes are invariably extremely difficult to identify and their prediction can only be based on a complete understanding of the chain of phenomena, from the displacement

cascade to the macroscopic response of the material to applied loads in the presence of radiation induced defects. The study and possibly prediction of all the steps along this chain, by means of, mostly, computational tools, is what is generally referred to as *multiscale modelling* and makes use of techniques spanning from quantum mechanical (*ab initio*) calculations, to, in principle, dislocation dynamics, going through molecular dynamics and Monte Carlo algorithms. Some of these techniques will be briefly introduced in what follows. Since little work of multiscale modelling type has been so far performed on Fe-Cr systems, we started off from the basis, i.e. by doing *ab initio* calculations, which are necessary to expand and complement the database of basic properties of the alloy known from experimental measurements. Some of the relevant *ab initio* results have already been published [32]. Others have been recently calculated using the same approach described in [33,34], but are still unpublished. *Ab initio* data are extremely important because they are often the most reliable estimate available for magnitudes that cannot be measured in experiments, such as defect binding energies and other defect features. The main limitation of *ab initio* techniques is that they cannot treat too large systems, since the method is very time consuming.

In order to increase the size of the system to be studied, classical molecular dynamics can be used. In essence, MD is an algorithm to follow the time evolution of a set of interacting atoms, by integrating their classical equations of motion, using adequate techniques for the calculation of the interatomic forces and convenient conditions for the control of the thermodynamical variables, such as temperature and pressure [35]. With MD we can currently simulate the behaviour of up to a few million atoms. The core of the technique, where all the physics of MD is contained, is the many-body interatomic potential used to describe the forces acting between the atoms. This is more and more often fitted empirically on data coming from *ab initio* calculations, so that in a way the interatomic potential can be looked at as the link to bridge small scale *ab initio* to larger scale MD simulations.

The work reported here consists mostly of MD simulations. All of them have been performed using Embedded Atom Method (EAM) [18] and Finnis-Sinclair (FS) [19] empirical interatomic potentials for Fe-Cr, which were fitted on both *ab initio* data and experimental results taken from the literature, as explained in [36] for the EAM and [37] for the FS. In fact, four EAM interatomic potentials for Fe-Cr systems were used, which differ essentially only for the value of alloy mixing enthalpy and bulk modulus on which they were fitted, as will be explained in section 4.

Along the multiscale modelling chain, MD still occupies a very basic (atomistic) level. Phenomena such as the formation of complex defects (e.g. voids or precipitates) by diffusion of point defects occur on too long timescales for MD to be of any use. To study this type of processes larger scale tools are needed. Kinetic Monte Carlo (KMC) codes offer the advantage, compared to analytical methods like rate equations [38,39], of retaining the detail of the spatial distribution of radiation induced defects, thereby being a kind of natu-

ral extension of MD studies. As will be discussed in the relevant section, KMC codes can both give an atomistic description (atomistic, or lattice, KMC [40–42]) or give up the atomic detail and treat only defects (object KMC [43–47]). In both cases, some external parameters need to be introduced in the model, coming either from *ab initio* or MD calculations, or from experiments. In this work, the KMC calculations that could be performed without the knowledge of many parameters have been executed and will be reported.

3 *Ab Initio*

Ab initio calculations have been carried out within the framework of density functional theory. The Kohn-Sham equations were solved using the Green's function technique by expanding the one-electron wave function in a basis set of exact muffin-tin orbitals (EMTO) [48–50]. The self-consistent one-electron potential and density are obtained within the local density approximation (LDA) [51]. Using the LDA charge density, the total energy is then calculated using the general gradient approximation. The problem of substitutional disorder in the Fe-Cr system is treated within the coherent potential approximation (CPA), which is known to give reliable electronic structure and total energies of completely random alloys [52–54]. A more detailed description of the *ab initio* approach and the results obtained will be found in [32].

The EMTO calculated mixing enthalpies of both paramagnetic and ferromagnetic Fe-Cr are displayed in Fig.1. The calculated mixing enthalpy for paramagnetic bcc Fe-Cr coincides with the experimental data (it is expected that the mixing enthalpy is independent of temperature, beside the effect of change in magnetic structure). As for the ferromagnetic alloy, for which no experimental measurements are available for comparison, note the minimum at small Cr concentrations and the transition from negative to positive at about 6% Cr. This complex behaviour, which is consistent with the observation of repulsive short-range order at small concentrations (<5% Cr) in Fe-Cr alloys [55], is expected to be difficult to reproduce with an empirical potential. However, a correct prediction of the stability of ferromagnetic Fe-Cr alloys as a function of Cr content, which is related to the mixing enthalpy, may be a key to understanding the Cr-rich phase separation observed in high Cr steels and must therefore be reflected in the most correct way when fitting EAM potentials for this alloy. This point will be further discussed in section 4 and in the whole report.

Other *ab initio* data (by C. Domain, EDF, [56]) will be presented in the following sections. They were obtained using the VASP (*Vienna Ab initio Simulation Package*) code [57–59], with a plane wave and pseudo-potential formalism. The

pseudo-potentials used to describe the electron-ion interaction are fully non-local Vanderbilt-type ultrasoft pseudo-potentials. The calculations were done within generalised gradient approximation (GGA) with the spin polarised and the plane cutoff energy was 240 eV. The supercell approach with periodic boundary conditions was used to simulate point defects as well as pure phases energetics. The defect calculations were performed at constant volume, thus relaxing only the atomic position in a supercell dimensioned with the equilibrium lattice parameter for Fe (2.8544). The calculations were done with 54 atom supercells with a Brillouin Zone (BZ) sampling of 125 k-points. The ion relaxations were performed using the standard conjugate-gradient algorithms implemented in the VASP code. More details about how the reported VASP calculations were performed can be found in [33,34].

The available set of *ab initio* calculations has given us the possibility to first fit and then check a series of new potentials for the Fe-Cr system. The fitting procedure is shortly outlined in section 4. The validation work is presented in section 5 (particularly 5.3).

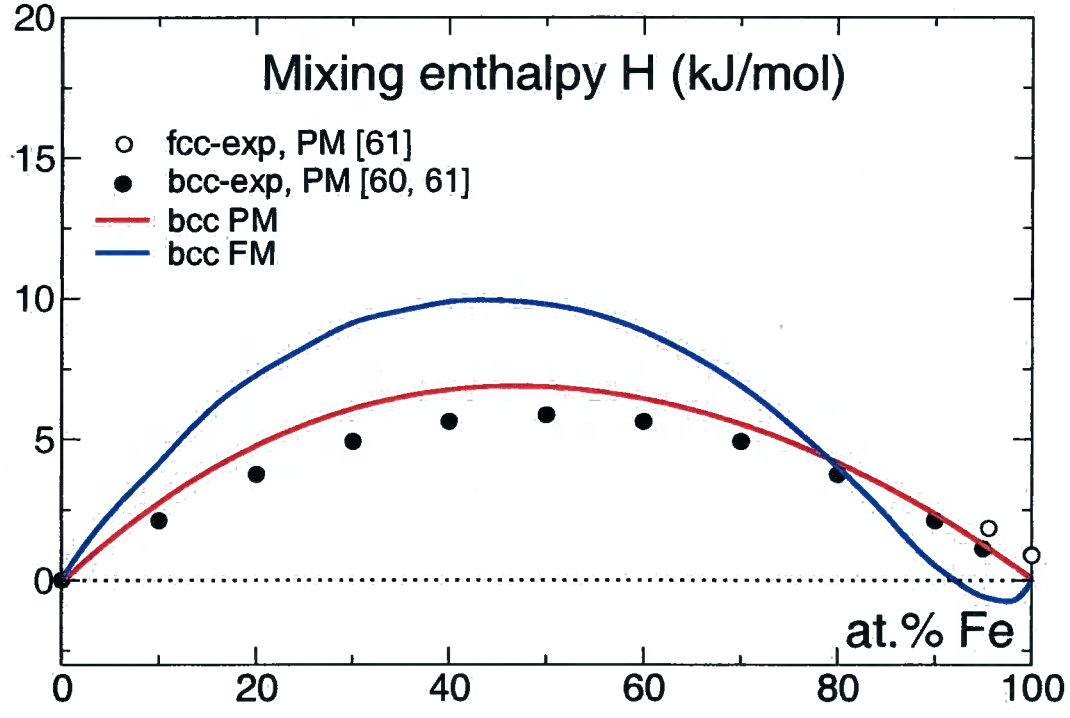

Fig. 1. The EMTO calculated mixing enthalpy of Fe-Cr as a function of Fe concentration, compared to available experimental values from [60,61] (only for the paramagnetic alloy).

4 Potentials

The series of Fe-Cr potentials used in this work were fitted using either the EAM [18] or the Finnis-Sinclair [19] formalism. These formalisms, though conceptually different, are in practice very similar and differ only for some mathematical subtleties. In both the total energy of the system of n atoms is written as a sum over the individual atomic energies:

$$E_{\mathrm{tot}} = \sum_{i=1}^{n} E_i = \sum_{i=1}^{n} \left[\frac{1}{2} \sum_{j=1}^{n} \Phi(r_{ij}) + F(\rho_i) \right], \tag{1}$$

where $\Phi(r_{ij})$ is the pairwise (electrostatic) interaction between atoms i and j; the function $\rho_i = \sum_{j \neq i} \rho(r_{ij})$ represents the electron density of the host system with atom i removed and r_{ij} is the scalar distance between atoms i and j. $F(\rho_i)$ is the many body term, i.e. the quantum mechanical energy required to embed atom i into a homogeneous electron gas of density ρ_i. It is mainly the way this density is defined that determines the difference between EAM and FS approach [19,18]. Because the electron density depends only on scalar distances to neighbouring atoms, the many body term here has no angular dependence. The curvature of F may be interpreted in terms of the traditional chemical bonding concept, where a new bond increases the total bonding energy but decreases the average energy per bond. In this context, ρ_i becomes a measure of the total bond order and $\rho(r)$ is a bond sensor. The weakening of successive bonds corresponds to a positive curvature of F:

$$\frac{\partial^2 F}{\partial \rho^2} > 0. \tag{2}$$

The procedure followed to fit the EAM potentials used in this work is described in [36], while for the FS potential the reference is [37].

All potentials have been further modified at short distances to smoothly transform into the Born-Mayer potential and then the universal screened Coulomb potential of Ziegler, Biersack and Littmark [23], following the procedure described in [15].

Four EAM Fe-Cr potentials were fitted, using the set of fitting parameters listed in table 1.

The first potential, in chronological order, was fitted to an experimental mixing enthalpy value, measured at high temperature, in a range where Fe-Cr alloys lose their magnetism (see figure 2 for details) and should thus be appropriate to describe "*paramagnetic*" (PM) Fe-Cr. In particular, the experimental

Table 1
Fitting parameters for the different EAM potentials. The only difference is the value of bulk modulus, lattice parameter and mixing enthalpy for the alloy, chosen as described in the text.

	FM-5	FM-10	PM-10	FM-20
$E_{coh}^{Fe}(eV)$	-4.28	-4.28	-4.28	-4.28
$B^{Fe}(kbar)$	1730	1730	1730	1730
$a^{Fe}(\mathring{A})$	2.866	2.866	2.866	2.866
$E_{fnr}^{V_{Fe}}(eV)$	1.60	1.60	1.60	1.60
$E_{coh}^{Cr}(eV)$	-4.10	-4.10	-4.10	-4.10
$B^{Cr}(kbar)$	1910	1910	1910	1910
$a^{Cr}(\mathring{A})$	2.87	2.87	2.87	2.87
$E_{fnr}^{V_{Cr}}(eV)$	1.90	1.90	1.90	1.90
$E_{coh}^{Fe-Cr}(eV)$	-4.271	-4.262	-4.262	-4.244
$B^{Fe-Cr}(kbar)$	1593	1544	1544	1664
$a^{Fe-Cr}(\mathring{A})$	2.866	2.866	2.866	2.866
$H^{Fe-Cr}(meV)$	**-5.91**	5.16	21.85	41.39

mixing enthalpy and bulk modulus for 10%Cr were used as fitting parameters. This potential is hence denoted as PM-10.
The paramagnetic phase, however, is a high temperature phase that a reactor material would not be heated to under operation. For this reason, in the light of the significant difference between *"ferromagnetic"* and *"paramagnetic"* mixing enthalpies, especially for low Cr concentrations (see figure 1), three *"ferromagnetic"* potentials were fitted as well, using the EMTO calculated values of mixing enthalpies for the ferromagnetic alloy, shown in figure 1, and corresponding bulk moduli and cohesive energies.
The reason for fitting three potentials was that each potential can only be fitted to the mixing enthalpy and bulk modulus values corresponding to one particular Cr concentration. As is shown in section 5.3, it is impossible to reproduce in this way the complex behaviour of the "ferromagnetic" mixing enthalpy shown in figure 1. Therefore, a possible solution to this problem was identified in the fabrication of potentials for different Cr concentrations. The present report becomes therefore an exploratory study to assess the possible advantages of creating a *concentration-dependent* potential. The three potentials are denoted as FM-5, FM-10 and FM-20, with explicit reference to the Cr concentration mixing enthalpy, bulk modulus and cohesive energy values used for the fitting procedure. Note that the lattice parameter was considered to be the same for all concentrations. Note also that, in accordance with figure 1, the mixing enthalpy for 5% Cr to which FM-5 was fitted is negative.

One important observation about these Fe-Cr potentials is that the Cr-Cr component was taken unmodified from the literature [62] and is known not to be able to correctly reproduce all elastic properties of pure Cr. Therefore, the Fe-Cr potentials are used here only in a region of relatively low Cr concentrations (up to a maximum of 20% Cr), which are the ones of interest to model steels. The inadequacy of the Cr-Cr contribution may prevent a correct description of phase separation.
The FS potential was fitted by Konishi and co-workers and is currently being used for the simulation of surface Cr induced displacement cascades in Fe [63]. The results reported here for this potential have been kindly provided by F. Chami (U. of Sheffield) [64] and will be denoted as FS-II. In addition, values calculated using the Fe-Cr EAM potential by Farkas and co-workers [62] will be also reported for comparison.

5 Molecular Dynamics

The MD code used in this work is DYMOKA, an enriched version of the older code CDCMD, now known as XMD [65], originally written by John Rifkin at the University of Connecticut. CDCMD has been upgraded into DYMOKA by EDF and the University of Lille in France [22].
The MD technique was developed originally for the study of liquids [66–68],

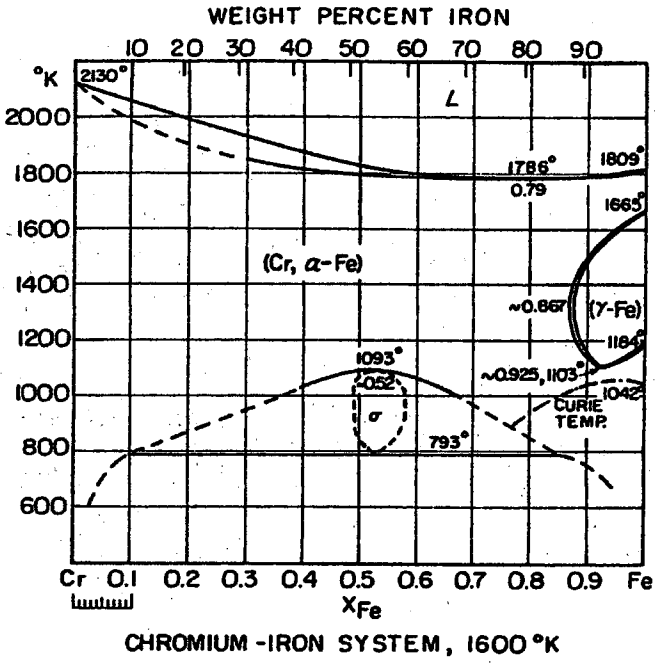

Fig. 2. Phase diagram of Fe-Cr as a function of temperature and Fe concentration. Taken from Hultgren *et al.* [61]

but it became soon equally important for the study of solids, the first application, at an embryo stage, in this field being the simulation of displacement cascades [69]. Nowadays, MD is applied to the study of the most different systems: from crystals to amorphous, from surfaces to bulk, including the presence of defects and impurities [70]. What makes MD superior to other numerical techniques is its inherent capability of dealing with systems too complex to be modelled using any analytical approach, without the need of introducing any simplifying hypotheses or approximations (except, that is, in the cohesion model used to determine the interatomic forces), the only real limit to its capabilities being the computational cost of the simulation. Still, there is a large number of key phenomena in materials taking place on a timescale at reach for MD. In particular, the production of radiation damage in displacement cascades is known to occur within a few picoseconds.

5.1 Method

Molecular dynamics uses Newtonian mechanics to calculate timestepwise the dynamical evolution of a system of particles. An interatomic potential defines the interaction strength between the atoms. A system is initially constructed with points defined by three co-ordinates in a real space box, distributed according to a certain crystallographic structure. These points can then be attributed to atoms (virtual atoms). The space available for calculation is the real space in the box. The boundary conditions can be set to either reflective, fixed or identification of opposite sides (so called *periodic boundary conditions*, PBC). With PBC we get virtually an infinite simulation box. The timestep is defined by the user and the atoms are initially given random velocities, based on the temperature of the system. At each timestep, the equations of motion are solved and the atoms are moved accordingly. For more details see e.g. [35]. It is often useful to know what configuration, and with what total energy, a system of virtual atoms containing e.g. defective structures can be *frozen* into, by quenching the system to a temperature of 0 K. To do this there are different methods. A frequently used one is to set the velocity of each atom to zero if the scalar product of the velocity and the acceleration is negative. This is based on the observation that, in such a case, the atom is moving away from its local energy minimum and forcing the velocity to vanish will quickly lead it to its equilibrium position, compatibly with the other atoms surrounding it. This is the method we used in this work. This type of calculations are often referred to as molecular *statics* (MS), in spite of the fact that the quenched state is reached dynamically in this case.

5.2 *Definitions*

MD provides in a natural way the cohesive energy of an atomic configuration, calculated from the adopted interatomic potential. Defect formation energies, binding energies, migration energies, *et cetera*, can be deduced from this information, and all is needed for this purpose is to figure out how to manipulate the system and what cohesive energies to compare to find the desired energy value.
A very important point to remember when calculating energy properties of atomic systems is the need to be consistent. For example, care must be taken to make sure that the exact same alloy (that is, the same atomic configuration surrounding the region of interest) is compared before and after the manipulation of the system (for example when adding an interstitial or a vacancy). This problem is particularly delicate in non-diluted alloys, where the local concentrations of solute atoms play a very important role and can greatly modify the result. The only way this effect can be cancelled out is by ensuring that the same system matrix around the defect is maintained before and after the manipulation. Effects of changing configurations at constant solute atom concentrations must be taken into account by averaging on the results obtained from different random configurations. The simulations, in addition, have to be done with a constant sized simulation box. We calculated formation, binding and migration energies mostly and will now shortly describe the definitions used. All calculations were done at 0 K.

5.2.1 *Formation energy*

The formation energy of any kind of object inserted into a predefined lattice, be it a pure Fe matrix or an alloy, is the following:

$$E_f^X = N\left(E_{coh}^{rlx}(X) - E_{coh}^{rlx}(ref)\right) \tag{3}$$

where $E_{coh}^{rlx}(X)$ is the cohesive energy of the relaxed system with the object X inserted and $E_{coh}^{rlx}(ref)$ is the cohesive energy of the relaxed reference system, generally the crystal alloy at equilibrium, without defects. N is the number of atoms in the simulation box, including the inserted object (e.g. N is the number of lattice sites plus or minus 1 in the case of, respectively, a self-interstitial atom or a vacancy). If solute atoms are included in object X, the reference state must take this into account. For example, the substitution energy of a solute atoms is calculated as:

$$E_s^{SA} = NE_{coh}^{rlx}(SA) - (N-1)\,E_{coh}^{rlx}(Fe) - E_{coh}^{rlx}(SA) \tag{4}$$

where SA stands for solute atom and $E_{coh}^{rlx}(SA)$ is the cohesive energy of the pure species present as solute atom in the Fe matrix (e.g. bcc Cr). In MD, these calculations are coded by setting up the initial atomic matrix and relaxing it, using the quenching algorithm described in 5.1. This provides the value for $E_{coh}^{rlx}(fm)$. Then the object X is inserted without touching the atomic distribution in the alloy and the system is relaxed again, the end result being $E_{coh}^{rlx}(X)$.
For the formation of vacancies we do not expect the relaxation to be very dramatic and therefore it is customary to use a timestep of one femtosecond (typical MD timestep value). For the formation of interstitials, or more complex structures, the distortion of the neighbouring atoms is substantial and therefore it is safer to take a shorter time step, at least in the initial phase of the relaxation.

5.2.2 Binding energy

The binding energy of a composite object can be defined in two ways. Either as the difference in the energy of the system with the parts of the object being far separated, to the energy of the system with the composite object formed and relaxed. Or as the difference of the sum of the formation energy of the parts to the formation energy of the composite object. In formulae:

$$E_b^{XY} = \begin{cases} N\left(E_{coh}^{rlx}(X \text{ far from } Y) - E_{coh}^{rlx}(XY)\right) \\ E_f(X) + E_f(Y) - E_f(XY) \end{cases} \tag{5}$$

The first definition of binding energy is more adherent to the physical processes the binding energy should quantify (i.e. dissociation of defect clusters), but if it is used care must be taken to ensure that no interaction exists between the two objects in the reference case. The second one is often more practical as it spares one simulation. Both of them yield a positive value whenever a bond exists, i.e. whenever the system finds it energetically more favourable to have the two objects forming one complex, rather than being separated (in some papers the opposite convention is used: conceptually the two are equivalent, but the convention used must be stated). Since both definitions should lead to the same result, this can be checked by using both. For example, the binding energy between two vacancies was calculated as the difference of two times the formation energy of the vacancy to the formation energy of the system with two nearby vacancies, and also as the difference of the formation energy of a system containing two non-interacting vacancies, to the formation energy of the system with two nearby vacancies.

5.2.3 Migration energy to vacancy

The migration energy of an atom can be defined as the energy difference between the initial state (the atom in its crystal lattice position) and the maximum energy state along the least energy migration path (the path to the first nearest neighbour vacancy), that is, the energy at the saddle point of the transition leading to the exchange between the atom and the neighbouring vacancy. The energy barrier for migration can therefore be calculated as:

$$E_m^X = E_{coh}^{rlx}(saddle\ point) - E_{coh}^{rlx}(initial) \tag{6}$$

Generally the determination of the saddle point of a transition is not an easy task. In the case of a simple vacancy jump, however, this can be done in MD by artificially approaching an atom towards a vacancy along the shortest segment joining the two lattice positions. At each intermediate position, the atom is constrained on a plane orthogonal to the trajectory, i.e. it cannot regain its equilibrium position. However, all positions on the plane are allowed and the relaxed energy is calculated at each intermediate position. The maximum energy value obtained by this method is postulated to correspond to the saddle point energy.

The migration energy is an important parameter to be calculated because in principle it can be compared with experimental values, obtained by diffusivity studies. However, in those studies the magnitude that is measured is an activation energy that equals the sum of the vacancy formation energy and the migration energy as calculated using the above described method:

$$E_a^X = E_f^v + E_m^X \tag{7}$$

It is this sum that can be compared to experimental data.

5.3 Results

The first check regarded the lattice parameter at 0 K as a function of concentration (see figure 3). This calculation was set up in MD by doing relaxed iterations over an increasing lattice parameter and checking for the one that gives the lowest energy for random solutions of increasing Cr concentration. Although both *ab initio* and MD calculated values oscillate more than the experimental ones, the difference is very small, probably below the experimental error, and the essential constancy of the lattice parameter over the explored concentration region is rather well reproduced by both MD and EMTO. The only outlier is the potential by Farkas and co-workers, that predicts a contin-

uous growth, like the experimental values, but well above the other curves.

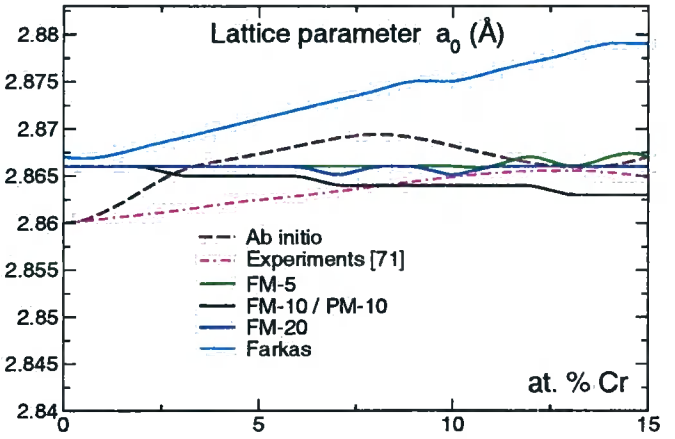

Fig. 3. EAM lattice parameters versus concentration as compared to *ab initio* and experimental ones. The potentials reproduce the correct values with only a small error.

Secondly, the mixing enthalpy was calculated as a function of Cr concentration (see figure 4). It can be seen that the EMTO (and therefore experimental) paramagnetic mixing enthalpy versus Cr concentration is well reproduced by the PM-10 potential, while the Farkas potential curve is well above the other, although in principle fitted to the same heat of mixing [62]. The non-monotonous behaviour of the ferromagnetic mixing enthalpy is not correctly reproduced by any of the FM potentials. These match the *ab initio* curve only in the neighbourhood of the concentration for which they were fitted, generally with the wrong slope. The idea of creating potentials for different Cr concentrations (5%, 10% and 20%) stemmed exactly from this difficulty of reproducing the ferromagnetic mixing enthalpy behaviour versus Cr concentration with one interatomic potential. In principle, the FM-5 potential should be used in the negative enthalpy region, the FM-10 should work at intermediate concentrations, while the FM-20 should apply for larger Cr concentrations, where phase separation takes place according to the Fe-Cr phase diagram (see figure 2). However, since the general behaviour of the ferromagnetic mixing enthalpy is not properly reproduced in any concentration range by any potential, this scheme may prove more problematic than initially envisaged. Advantages and shortcomings of this *concentration-dependent* approach will be discussed in the conclusions. Globally, figure 4 shows that: PM-10 and FM-20 tend to behave in a similar manner, in the direction of increasing mixing enthalpy with growing Cr concentration; FM-5 goes in the opposite direction, while FM-10 is intermediate between the two trends. It will be seen that this general relationships hold true for most magnitudes calculated in this work.

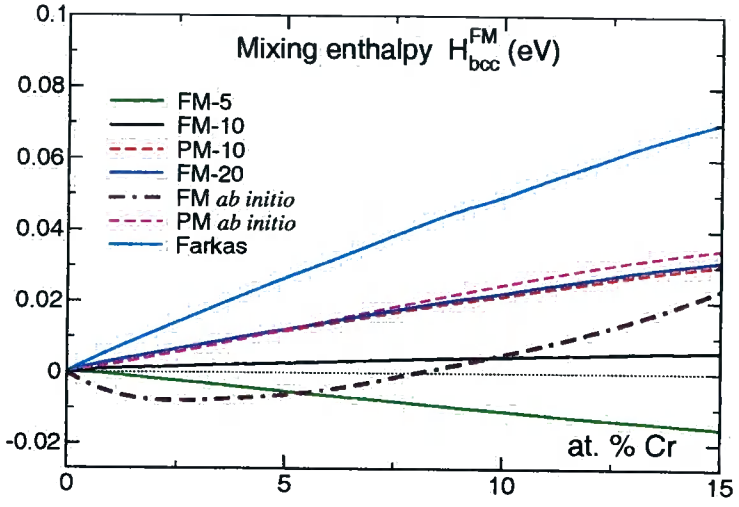

Fig. 4. The mixing enthalpy of the paramagnetic system calculated from MD using the PM-10 potential corresponds nicely to the experimental and *ab initio*. The ferromagnetic MD calculations with the FM potentials, on the contrary, are not able to reproduce the non-monotonic behaviour seen in *ab initio* calculations.

5.3.1 Vacancies and Cr atoms

After the initial tests reported above, we calculated formation and binding energies for defects, broadly including in this category also solute atoms. In this section, the results regarding vacancies and Cr atoms are presented.

In table 2 the results for the formation energy of a single vacancy and the substitution energy of a single Cr atom in an otherwise pure and perfect Fe matrix, obtained with different empirical interatomic potentials, are indicated and compared with available *ab initio* and experimental data. The computed vacancy formation energies in Fe are found to fall in the range of the reported experimental values, with the *ab initio* in the upper region of the experimental interval and the empirical potentials in the lower region. The Cr atom substitution energy is seen to be strongly dependent on which mixing enthalpy the potential was fitted to: it is twice as high for PM-10 and FM-20, as compared to FM-10, while - as expected - it is minimal for FM-5, the FS potential by Konishi *et al.* [37] predicting a value intermediate between these two. The Farkas potential predicts the highest substitution energy. These trends are not surprising, because for a regular solution the mixing enthalpy is given by the expression:

$$\Delta H_m = \Omega c(1-c) \tag{8}$$

where c is the solute concentration and Ω is the heat of solution, which in good approximation can be demonstrated to equal the substitution energy of a Cr atom in the Fe matrix. So, the slope of the mixing enthalpy curve versus Cr concentration at 0% Cr should correspond to E_f^{Cr}. For example, the experimental value for E_f^{Cr} indicated in table 2 has been assessed using the slope of the experimental curve of figure 1 at 0% Cr for the paramagnetic alloy, which exhibits a regular behaviour. The shape of the mixing enthalpy curve for the ferromagnetic Fe-Cr alloy clearly does not correspond to a regular solution. However, the interpretation of the initial slope as related to the substitution energy can be still considered valid. Therefore, the fact that FM-5 predicts a positive, though small, value for E_f^{Cr}, means that, for very small Cr concentrations, also this potential predicts a positive mixing enthalpy, the curve starting with positive slope and becoming very soon negative, so as to meet the fitting value of -5.91 meV at 5% Cr. Indeed, from figure 4 it can be guessed that the mixing enthalpy curve predicted by FM-5 does have a negative curvature and an initial positive value. Again identifying the slope of the mixing enthalpy curve at 0% Cr with E_f^{Cr} also in the ferromagnetic case, the EMTO value for the substitution energy can be assessed and is found essentially to agree with the VASP value, although more refined (more k-points) EMTO calculation are in progress to confirm or deny this agreement.

Table 2
Formation energies of single vacancy E_f^V and substitution energy of a Cr atom E_s^{Cr} in a pure Fe matrix, according to different empirical interatomic potentials, compared with *ab initio* calculations. The EMTO value is derived from figure 1.

(eV)	E_s^{Cr}	E_f^V
FM-5 EAM	0.050	1.543
FM-10 EAM	0.227	1.543
PM-10 EAM	0.415	1.543
FM-20 EAM	0.418	1.543
EAM (pure Fe) [21]		1.56–1.63
FS-I [37,64]	0.158	1.80
FS-II (pure Fe) [72]		1.70
EAM Farkas	0.703	1.63
VASP [33,56]	-0.354	1.95
EMTO (fig. 1)	-0.384	
Experiments	0.224 (PM)	1.53–2.2 [73–77]

The concentration dependence of the vacancy formation energy was also calculated (see figure 5) by removing an Fe atom from random alloys of growing Cr concentration and calculating the cohesive energy difference before and

after removal (at constant number of atoms). The calculation for each concentration was repeated with different random alloys, checking also that the local concentration around the vacancy corresponds to the wanted concentration, and the average values were retained for each concentration. It turns out that the addition of Cr to the system generally decreases the vacancy formation energy. This result can be rationalised by observing that in average the formation energy will be decreased by an amount proportional to the V-Cr binding energy and to the Cr concentration. Intuitively, the formation energy of the vacancy should decrease more or less linearly with the Cr concentration, any departure from linearity being a sign of a dependence on concentration of the V-Cr binding energy (always assuming random distribution of Cr atoms). The slope of the line should bear some relation with the strength of the V-Cr *bond* for a dilute solution. Indirectly, therefore, we are led to believe that the V-Cr binding energy is higher according to FM-20. The *jumps* exhibited by the points in the graph have to be related to the forcibly discrete change in the number of Cr atoms around a vacancy with growing Cr concentration.

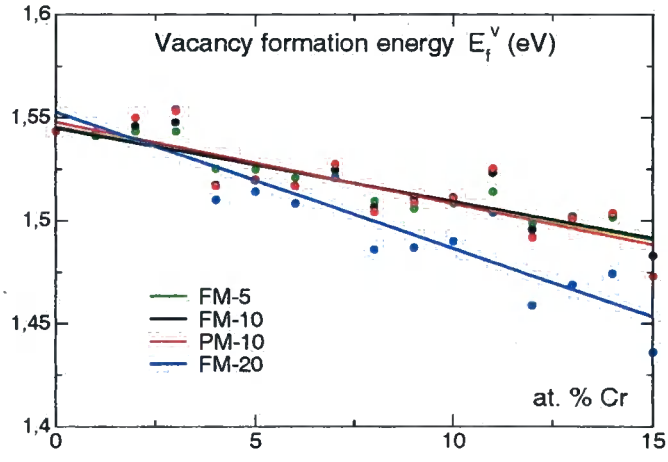

Fig. 5. The concentration dependence of the vacancy formation energy.

The tendency of Cr to segregate can be assessed by calculating the binding energy of the solute atoms with vacancies and with themselves. Some data of this type are available also from *ab initio* calculations [56]. The comparison between these results and those obtained using the Fe-Cr empirical potentials is given in table 3.

The binding energy of the second nearest neighbour divacancy is always higher than the first nearest neighbour divacancy. In spite of the lack of experimental data of divacancy binding energy in Fe, theoretical analyses suggest that this is indeed a feature of bcc transition metals [78] and has been measured to be so in the case of Mo [79].

The values of the V-Cr binding energies vary from one method to the other, but the basic fact that Cr atoms are not, or only very weakly, bound to vacancies

emerges clearly, the Finnis-Sinclair potential by Konishi *et al.* [37] labelled as FS-I being, in this case, the closest to *ab initio* results, as it predicts a repulsion between V and Cr at 2^{nd} nearest neighbour distance. Note that the strength of the V-Cr *bond*, though always small, increases with the mixing enthalpy value to which the EAM potentials were fitted, possibly as a consequence of the growing *repulsion* between Fe and Cr atoms. Indeed, the Farkas potential, which predicts the highest mixing enthalpy (figure 4), predicts also the largest V-Cr binding energy (0.1 eV). This trend is also in qualitative agreement with the indirect assessment of the V-Cr binding energy from figure 5.
This negligible interaction between Cr atoms and vacancies is consistent with a series of data found in the literature. Demangeat calculated, using a full-electron method, the V-Cr binding energy to be in any case below 0.089 eV [80]. According to a positron annihilation assessment of the onset of vacancy migration in pure Fe and Fe-Cr, no difference was found between the two materials [81]. It is also known that the diffusivity of Cr in Fe is extremely close to the self-diffusivity of Fe, in a large range of Cr concentrations [82], a sign of negligible V-Cr binding energy. Finally, muon spin rotation measurements by Möslang and co-workers showed that the V-Cr binding energy in Fe is in any case less than 0.1 eV (below the resolution of the method) [83].
For both V-V and V-Cr binding energies calculations are in course to assess a possible dependence on solute concentration.
Turning to Cr-Cr interaction, the discrepancy between empirical potentials and *ab initio* becomes more significant. No interatomic potential predicts a repulsion between Cr atoms as strong as is found with VASP. In addition, when an attractive behaviour is found, the strength of the interaction is seen to grow with the value of the mixing enthalpy to which the potentials were fitted. This behaviour was to be expected, because a growingly positive mixing enthalpy clearly forces the system to phase separation. Since this separation does not take place at low Cr concentrations, the potentials fitted to positive mixing enthalpies should not be used for very small Cr concentrations, as is the case of these calculations, where only a few Cr atoms are introduced in the system. FM-5 is the only potential that is being used, roughly speaking, in its range of application, and yields negative binding energy values between Cr atoms, together with, in some cases, the potential by Konishi and co-workers [37]. However, the repulsion is always softer than according to VASP.

In figure 6 the binding energy of larger and larger clusters of Cr atoms is graphically represented. Here the different behaviour between the four EAM potentials becomes patent. We find a saturation of the binding energy with increasing cluster size for the FM-10 potential: this indicates that, although the formation of large Cr clusters is in principle possible, the growth may in this case stop to around 10 atoms, since there is no energetical advantage in building larger clusters. For the FM-5 potential, in accordance with the negative mixing enthalpy value to which it was fitted, we see instead an increasing repulsion for larger complexes, indicating a tendency to force the alloy into

Table 3
Binding energies involving vacancies and Cr atoms.

(eV)	FM-5	FM-10	PM-10	FM-20	EAM Farkas	FS-I [64]	VASP [34,56]
$E_b^{V-V}(1nn)$	0.19	0.19	0.19	0.19	0.16	0.15	0.14
$E_b^{V-V}(2nn)$	0.21	0.21	0.21	0.21	0.21	0.21	0.28
$E_b^{V-Cr}(1nn)$	0.031	0.035	0.052	0.070	0.10	0.024	0.029
$E_b^{V-Cr}(2nn)$	0.024	0.051	0.059	0.065	0.042	-0.042	-0.01
$E_b^{Cr-Cr}(1nn)$	-0.001	0.005	0.034	0.031	0.009	0.026	-0.329
$E_b^{Cr-Cr}(2nn)$	-0.023	0.024	0.043	0.055	0.024	-0.030	-0.197
$E_b^{Cr-Cr}(3nn)$	0	0	0	-0.003	0	0.008	
$E_b^{Cr-Cr-Cr}(1nn)$	-0.051	0.016	0.099	0.092	0.016	0.057	-0.79
$E_b^{Cr-Cr-Cr}(2nn)$	-0.046	0.047	0.086	0.109	0.047	-0.013	
$E_b^{Four\ Cr}(1nn)$	-0.102	0.031	0.197	0.182	0.54	0.097	-0.97

some degree of order (equally spaced Cr atoms). This is in agreement with the experimental finding of repulsive short-range order in Fe-Cr alloys with less than 5% Cr [55]. The PM-10 and the FM-20 potentials behave basically in the same way, showing - as expected - increasing binding energy with the number of Cr atoms in the cluster. This indicates that these two potentials should be able to predict phase separation at high Cr concentrations, in accordance with experiments [30]. On the other hand, a too strong tendency to Cr atom aggregation cannot be accepted, because the α' phase is Cr-rich and not pure Cr. These issues will be further discussed in section 6. Note that the Farkas potential predicts an even stronger attraction between Cr atoms in cluster. Note, however, that all of these potentials are being pushed well above their validity range when treating large Cr clusters, as a consequence of the non completely correct description of the elastic properties of pure Cr inherent to the used Cr-Cr term.

5.3.2 Self-interstitials and Cr atoms

The formation energy of different interstitial configurations, including solute atoms, is another important issue to be checked. The interstitial configuration with the lowest formation energy is going to be the most stable and therefore the most frequently encountered in simulations performed with the corresponding potential. Experiments tell us that the most stable interstitial configuration in pure bcc metals is the $\langle 110 \rangle$ dumbbell [84–86]. Other possible configurations, energetically close to the most stable one and typically considered in bcc metals are the $\langle 111 \rangle$ dumbbell and the $\langle 111 \rangle$ crowdion. It is known that EAM interatomic potentials can predict either the $\langle 110 \rangle$ or the $\langle 111 \rangle$

dumbbell configuration to be the most stable in Fe, depending on the range of the potential [21]. The EAM potentials used in this work, being descendants of Simonelli's long-range one [21], predict accordingly the ⟨111⟩ configuration to be the most stable (see table 4), in disagreement with the experimental evidence, as well as VASP calculations [33]. The reason for this wrong prediction has been found to be that the gradient of the potential at distances around 2Å is too low. For example, both Ackland's potential [72], which is of Finnis-Sinclair type, and Simonelli's short-range EAM successfully reproduce the ⟨110⟩ dumbbell as the lowest energy configuration and have much higher gradient at this distance, which is the expected one between the atoms in the dumbbell. It is therefore hoped that this shortcoming of the present Fe-Cr potentials can be removed through moderate stiffening in the appropriate range. Work is in progress on this issue.

The main effect of predicting the ⟨111⟩ dumbbell orientation to be more stable than the ⟨110⟩ should be an underestimation of the migration energy of single SIA in pure Fe. Indeed, the currently accepted SIA migration mechanism is based on the idea of athermal glide along the ⟨111⟩ direction, via ⟨111⟩ crowdion formation, with frequent ⟨111⟩ direction changes, giving rise to effective 3D motion [41]. According to this picture, the bottleneck for migration, which eventually determines the migration energy of single SIA, is the rotation from the most stable ⟨110⟩ orientation to the less stable ⟨111⟩ orientation, the only one that allows athermal gliding. Since, according to the EAM potentials used

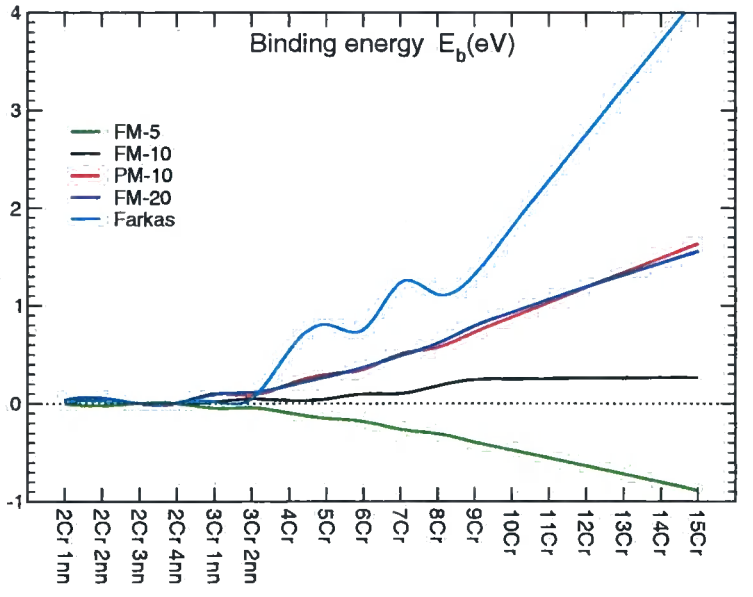

Fig. 6. The binding energy of Cr-complexes.

Table 4
The formation energy of interstitials. In parenthesis are values deduced from reported data.

(eV)	$E_f^{<110>}$ $(Fe-Fe)$	$E_f^{<111>}$ $(Fe-Fe)$	$E_f^{<110>}$ $(Fe-Cr)$	$E_f^{<111>}$ $(Fe-Cr)$	$E_f^{<110>}$ $(Cr-Cr)$	$E_f^{<111>}$ $(Cr-Cr)$
FM-5	4.15	**4.02**	3.81	**3.72**	3.67	**3.64**
FM-10	4.15	**4.02**	3.98	**3.92**	**4.00**	4.02
PM-10	4.15	**4.02**	4.16	**4.10**	**4.32**	4.35
FM-20	4.15	**4.02**	4.80	**4.77**	5.16	**4.90**
EAM Farkas	3.66	**3.54**	4.31	**4.24**	4.57	**4.44**
FS-I [37]	(3.90)		4.55	unstable		
FS-II pure Fe [72]	**4.87**	5.00				
VASP [33]	**3.41**	4.11	(3.06)	**(2.70)**	(3.25)	**(2.67)**

in this work, SIA always lie on the ⟨111⟩ direction, their predicted migration energy is expected to be negligible, so that they will be in fact moving very fast, faster than they should, at any temperature. It should be noted that this problem is not shared by Konishi's potential [37], which is a short-range one of Finnis-Sinclair type.

Whatever about SIA migration in pure Fe, from table 4 it can be seen that FM-5 and FM-10 predict the mixed Fe-Cr crowdion to be more stable than any pure Fe-Fe dumbbells, in agreement with VASP results. In addition, again in agreement with VASP, all the EAM potentials predict the Fe-Cr ⟨111⟩ crowdion configuration to be more stable than the ⟨110⟩ dumbbell. This agreement is all the more important because no information about interstitial atoms was used as fitting parameter. The FS potential by Konishi *et al.* [37] seems to be out of scope in this case, at least in comparison with *ab initio* data, as it gives the Fe-Cr ⟨110⟩ dumbbell as only possible stable configuration, with a formation energy higher than the Fe-Fe dumbbell. The PM-10 and FM-20 potentials, as well as Farkas potential, are also out of scope as they also yield a higher formation energy for the mixed configuration as compared to the Fe-Fe dumbbell.
It is noteworthy that, both with VASP and the two potentials FM-5 and FM-10, also the Cr-Cr dumbbell is found to have a lower formation energy than the Fe-Fe one, although only FM-5 predicts the ⟨111⟩ configuration to be of lower energy, in agreement with the *ab initio* results. These were originally given in terms of binding energies and these quantities are therefore reported in table 5. This table shows from a different point of view agreement and disagreement between VASP results and empirical potentials. Except FM-20 and Farkas, all EAM potentials predict a strong binding energy for a Cr atom in an interstitial configuration, in excellent agreement with the *ab initio* value

Table 5
Binding energy of Cr with interstitials. In parenthesis deduced values.

(eV)	FM-5	FM-10	PM-10	FM-20	EAM Farkas	FS-I [37]	VASP [56]
$E_b^{<110>(Fe-Cr)}$	0.257	0.266	0.273	-0.364	0.003	(-0.49)	-0.005
$E_b^{<111>(Fe-Cr)}$	0.349	0.333	0.338	-0.330	-0.067	unstable	0.358
$E_b^{<110>(Cr-Cr)}$	0.452	0.476	0.531	-0.307	0.376		-0.548
$E_b^{<111>(Cr-Cr)}$	0.482	0.455	0.503	-0.042	0.506		0.035

(the best agreement is achieved with FM-5). The difference is that, according to VASP, the ⟨110⟩ mixed dumbbell configuration is unstable, while according to the EAM potentials it can subsist, although with higher energy than the ⟨111⟩. The potential by Konishi *et al.* gives reversed results. However, in the original paper by Konishi [37] calculations of binding energies of Cr atoms in different positions with respect to an Fe-Fe dumbbell were reported and positive values were found in some cases, so that, though in a different way, this potential too predicts an attractive interaction between SIA and Cr atoms in solution. The Farkas potential exhibits an even different behaviour, by predicting essentially no binding energy for the Fe-Cr dumbbells, but high stability of the Cr-Cr dumbbells. As a final observation on table 5, we shall note that, according to VASP, the Cr-Cr interstitial configuration is not as favourable as the empirical potentials yield, most likely as a result of the strong repulsion between Cr atoms in Fe, that none of the empirical potentials can reproduce.

From the experimental point of view, it has been already discussed in the introduction that an interaction between SIA and Cr atoms must exist in Fe-Cr alloys to explain the observed differences in loop accumulation under irradiation [27,28]. Moreover, the convergence of simulation results towards the stability of mixed dumbbells is supported by a resistivity study of recovery of low-temperature electron-irradiated Fe-Cr alloys [29], proving not only the existence of mixed dumbbells in these alloys, but also hinting at a high stability of Cr-Cr interstitial configurations.
In dynamical simulations performed with the FM-10 potential, pure Fe-Fe dumbbells gliding one-dimensionally along the ⟨111⟩ direction have been seen to stop as soon as they encountered a Cr atom, the latter remaining bound to the dumbbell and drawing the center of the interstitial configuration onto itself, thereby forming a crowdion. Therefore, according to this potential Cr atoms are traps for highly mobile SIA in Fe-Cr alloys and analogous results are expected from the FM-5 potential as well as, most likely, the PM-10. The mobility of the mixed interstitials, although not quantified yet, is consequently expected to be drastically lower than that of the SIA using these EAM potentials and probably also the potential by Konishi *et al.* would give a similar prediction [37]. To this regard, experimentally the situation is not completely clear, because from resistivity measurements Abe and co-workers

[87] estimated the effective migration energy of interstitials in Fe-10%Cr to be 0.4 eV, so higher than in pure Fe, while Maury and co-workers, also in a resistivity study, claim the mixed Fe-Cr dumbbell to move faster than the Fe-Fe dumbbells at low temperature [29].
The SIA migration energy in Fe is accepted to be experimentally close to 0.3 eV [88] and much lower (0.02 eV) in MD simulations (see e.g. [89]). This discrepancy between simulations and experiments is well-known and still not settled. It has been tentatively explained as the effect of unavoidable trapping impurities in real Fe, even when high purity Fe is used for the experiments, although some authors maintain that this underestimation of the SIA migration energy is a serious shortcoming of all existing empirical potentials for Fe. Recent *ab initio* results seem indeed to support the latter position [33], by finding a much higher energy difference between the ⟨111⟩ dumbbell configuration and the ⟨110⟩, thereby questioning the validity of the ⟨110⟩ to ⟨111⟩ rotation and ⟨111⟩ glide as migration mechanism. In this framework, it is not surprising that the potentials analysed in this work which, like all others, predict negligible SIA migration energy along the ⟨111⟩ direction and, at the same time, a high Cr-SIA binding energy, see Cr atoms as traps for SIA.

It can hence be concluded that, although not completely correct in the description of SIA in pure Fe, if we rely on VASP results and accept the experimental evidence and related uncertainties, the FM-5 and FM-10 potentials are probably at least qualitatively correct in the description of SIA in Fe-Cr alloys. On the contrary, PM-10, the potential by Konishi and, above all, FM-20, together with the potential by Farkas, seem to be less accurate in this case. About FM-20, though, it has to be stressed that the Cr concentration used for the reported calculations is a lot lower then the concentration for which the potential was fitted.

5.3.3 Migration energies

To complete the picture for the assessment of the validity of the proposed Fe-Cr interatomic potential, the migration energies are important properties to be calculated. This type of information is needed, for example, to perform atomistic kinetic Monte Carlo simulations using the simplest scheme: that of solute atom redistribution in an alloy via vacancy jumps (see section 6). It is long and widely accepted that vacancy diffusion jumps can only occur by exchange with first nearest neighbour atoms and that the study of a limited number of possible vacancy jumps around a solute atom is enough to provide a complete description of solute atom migration in bcc metals, at least in the case of dilute alloys [90]. These jumps are therefore traditionally used as a reference and for this reason have been considered here, in spite of the fact that we are not necessarily treating dilute alloys. Figure 7 shows the main relevant jumps, according to Le Claire's theory [90].

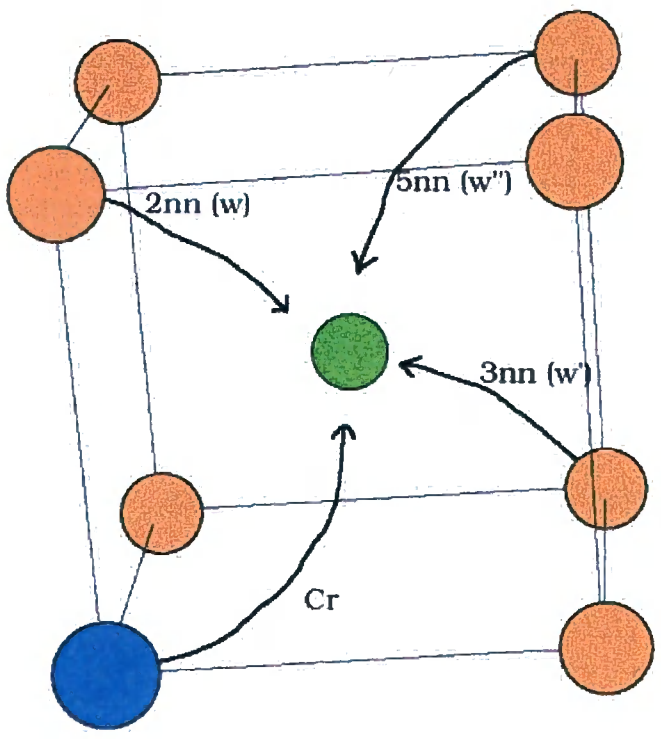

Fig. 7. The notations of the different migration paths. The yellow spheres are Fe atoms, the blue sphere is a Cr atom and the green is the vacancy. The nn-number refers to the Fe atoms' position relative to the Cr atom.

In table 6 the migration energies corresponding to the jumps of figure 7, calculated using the empirical interatomic potentials, are compared with *ab initio* results [56]. In table 7 the activation energies (equation 7) for Fe and Cr migration that can be deduced from the interatomic potentials and from VASP are compared with experimental data. The reported value for Cr atom diffusion corresponds to measurements in an alloy containing 12%Cr [82], which is the lowest concentration for which the diffusivity can actually be studied in a ferritic Fe-Cr alloy. It can be seen that the only significant discrepancy between the predictions of the empirical potentials and *ab initio* results is in the energy barrier for the jump of a Cr atom into the neighbouring vacancy: according to the empirical potentials Fe and Cr share essentially the same migration energy or, in the case of FM-20, the migration energy for Cr is higher than for Fe, while VASP yields a lower barrier from Cr than for Fe, as does the Farkas potential, although with a two times as big difference. A similar effect is seen when comparing activation energies to available experimental values. However, the comparison with experimental activation energies can be only indicative, since the values from the potentials and from VASP are sums of statically calculated energies and, in the case of the Cr atom, at vanishing Cr concentration, while the experimental values are obtained from Arrhenius plots and include the effect of impurities in Fe and a high concentration of solute atoms in Fe-Cr. Better conclusions about the performance of the po-

Table 6
Migration energy of Fe and Cr migration to a vacancy. The different symmetries are described in figure 7

(eV)	FM-5	FM-10	PM-10	FM-20	EAM Farkas	VASP [56]
$Fe \rightarrow V$	0.725	0.725	0.725	0.725	0.660	0.650
$Cr \rightarrow V$	0.698	0.728	0.706	0.941	0.456	0.580
$Fe \rightarrow V : w$	0.725	0.700	0.707	0.709	0.633	0.684
$Fe \rightarrow V : w'$	0.732	0.765	0.769	0.795	0.592	0.666
$Fe \rightarrow V : w''$	0.726	0.735	0.736	0.764	0.578	0.645

Table 7
Activation energy for Fe and Cr atom diffusion in Fe. The activation energy is obtained from the interatomic potentials as the sum of the migration and vacancy formation energy. In the case of Cr, the vacancy-Cr binding energy is subtracted [90]

(eV)	FM-5	FM-10	PM-10	FM-20	EAM Farkas	FS-II pure Fe [72]	VASP [56]	Exp.
$Cr \rightarrow V$	2.21	2.24	2.20	2.41	1.99		2.50	2.28 [82]
$Fe \rightarrow V$	2.27	2.27	2.27	2.27	2.29	2.48	2.60	2.60 [92]

tentials in describing Cr and Fe diffusion in Fe will be drawn after a full MD diffusivity study, currently in progress [91].

6 Kinetic Monte Carlo

Kinetic Monte Carlo (KMC) techniques are nowadays well established methods for the study of medium and long term evolution of radiation damage, up to timescales completely out of reach for MD [40–47]. The main limitation of these techniques is the still reduced volume of material that can be studied (lengthscale on the order of hundreds of nanometers at the most). In this section a general description of the method will be given and the results of applying an atomistic KMC approach to the study of Fe-Cr, always with a view to assessing the performance of the considered interatomic potentials, will be presented.

The prerequisite of any Monte Carlo method is that different events are possible in the studied system and to each of them a known probability can be assigned. In the case of radiation damage studies these events can be point defect migration, Frenkel pair annihilation, etc. Their probabilities can be normalised so that their sum is one. In this way, by extracting a random number between 0 and 1, one and only one of the possible events is chosen to happen: this correspond to a Monte Carlo step. The adjective *kinetic* is added to a MC algorithm whenever time is a variable that the method considers and can treat. The existing KMC algorithms may differ more or less significantly between them, but they are all based on the residence time algorithm introduced already in 1966 by Young and Elcock [93], which will be shortly described below. Broadly speaking, the existing KMC algorithms can be divided into two families: Atomistic KMC (AKMC) and Object KMC (OKMC). AKMC models retain the detail of the atomic-level description, i.e. the possible events involve a redistribution of atomic positions, including or not point defects and point defect clusters. AKMC models can be regarded as natural extensions of MD, in which not deterministic Newtonian mechanics, but stochastic statistical mechanics laws determine the evolution of the system [40–42]. All AKMC algorithms need to include a method to calculate the total energy of the system, because this magnitude is key in determining the probability of the possible events. For this reason, computing time may be an issue for these models: depending on different factors, the accessible timescales for AKMC methods may turn out to be limited and in some instances still far from macroscopically significant ones. This is why OKMC methods were worked out [43–47]: in this case the atomic detail is given up and the total energy of the system is not any more an important variable of the problem. The simulation treats not atoms but *objects* that can be anything: generally, in radiation damage studies, they are point defects, point defect clusters, solute atoms, impurities, traps, sinks, *et cetera*. Each object is defined by its type, size, centre-of-mass co-ordinates in space and reaction radius (i.e. the distance at which it interacts with other objects). The possible events are essentially migration of objects and reactions between objects. All possible reactions and migration modes must be known in advance and for each of them an activation energy and attempt frequency, or other parameters capable of suitably defining the relevant probability, need also to be known in advance. The advantage of OKMC approaches in terms of computing time is enormous: 40 years of irradiation in a power plant vessel can be simulated in a matter of a few days [47]. However, the amount of parameters needed in OKMC models is enormous as well, as it is easy to imagine, and the determination of the correct parameter set for a particular material is still an open question, for which no established methodology exists, although of course quite a lot of work has been done and tentative parameters for the description of radiation damage evolution at least in pure Fe have been

proposed by various groups and are available from the literature [44–47].

In the case of Fe-Cr systems there is no available parameter set to run OKMC simulations, not even at a tentative level, and work will have to be devoted to the calculation of at least the very basic parameters. It is easy to guess, from the results presented and discussed in this work, that the most important missing information is the diffusivity of SIA clusters in presence of Cr atoms, that are seen to act as traps and to easily form mixed dumbbells.

However, if an interatomic potential is available and the migration energy for solute atoms is acceptably well estimated, as is the case for Fe-Cr alloys, it is possible to run AKMC simulations on rigid lattice using the vacancy jump algorithm. In this AKMC approach the atoms are distributed on a rigid crystal lattice and the only type of defect that is introduced in the system and treated is the vacancy. The only possible physical process determining the evolution of the system is the exchange of position between an atom and a vacancy, located at first nearest neighbour distance, i.e. a diffusion jump. The energy of the system can be evaluated in principle in different ways, either using an empirical interatomic potential [42], or by introducing adequate pair interaction energy parameters [40], or a mixture of both approaches [41]. In our case, the first of the three possibilities is used. In this model the vacancy jump frequency for vacancy n and jump i is given by the Boltzmann expression:

$$\Gamma_{n,i} = \nu_{n,i} e^{-\frac{E_{m,n,i}}{kT}} \tag{9}$$

where E_m is the migration energy and ν is the attempt frequency. For every step, the probability of all possible vacancy jumps (8 for each vacancy in the bcc structure, except for vacancies belonging to vacancy clusters) is computed and one jump is then chosen randomly with the weight of that particular probability. Time is introduced in the system as the inverse of the sum of all the jump frequencies, for all the possible jumps of all the vacancies contained in the system, $\Gamma_{n,i}$, for each MC step:

$$\Delta\tau = \frac{1}{\sum_{n,i}\Gamma_{n,i}} \tag{10}$$

This correspond to the simplest form of Young and Elcock's residence time algorithm [93]. Note that, with this definition, the KMC timestep is a function of the jump frequencies, and therefore a function of the binding energies between solute atoms and vacancies predicted by the interatomic potential, as well as, of course, the choice of the attempt frequency. Therefore, the timestep cannot be controlled in the same way as in MD. Note also that the timestep length in equation 10 is an average over all possible jumps and does not contain only the event chosen to occur. In this way the length of the timestep is

kept more or less constant throughout the simulation. If the timestep was calculated as the reverse of the frequency of the chosen event, infrequent events would determine very long timesteps.

The only practical problem for the application of this algorithm is the determination of attempt frequency and migration energy for each possible jump. In principle, this is a difficult problem, because both these magnitudes are sensitive to the environment in which the jump takes place. In other words, strictly speaking a dedicated calculation should be executed for each local atomic configuration. Since this is computationally impractical, it is customary to introduce approximations. Thus, the attempt frequency is assumed to be a constant, on the order of the Debye frequency, i.e. $10^{13}s^{-1}$ (more precisely, the value $6 \cdot 10^{12}s^{-1}$ will be used in this work. The environment dependence of the migration energy can be heuristically treated according to many different models [40–42,93], none of them really justified by rigorous physical arguments. In this work, we adopted the same model as in [41] and [42], i.e.

$$E_m = E_0 + \frac{E_f - E_i}{2} \tag{11}$$

where E_0 is a constant energy barrier and E_f and E_i are the potential energies of the final and initial configurations, i.e. after and before the jump, calculated according to the interatomic potential. This model is a priori not better and not worse than any other, but it has the advantage of correcting a constant energy barrier according to the environment and, more specifically, the binding energy between vacancies and solute atoms predicted by a certain interatomic potential, so that this method is sensitive to differences between interatomic potentials. In addition, it is inherently biased to lead the system towards the lowest energy configuration, since the activation energy grows if $E_f > E_i$.

This AKMC scheme, although somewhat simplistic, is a very performant tool to simulate phenomena such as solute precipitation or segregation via a vacancy mechanism, both as a consequence of thermal annealing (equilibrium vacancy concentration) or irradiation (vacancy supersaturation). The simulation of these types of phenomena would be impossible by MD, both because the simulated timespan could never be long enough for a significant number of vacancy jumps to take place and because, in order to actually observe precipitation or segregation, systems containing millions of atoms should be considered. With an AKMC code, the evolution of a reasonably large system up to a macroscopically meaningful timescale, totally out of the scope of MD (seconds to hours) can be followed. It can therefore be regarded as a kind of *accelerated MD*, where the price to be paid, in order to extend the timespan

covered by the simulation, is to give up a correct description of the atomic interactions: no atomic oscillations and no relaxation around defects, or oversized solute atoms, or undersized interstitial atoms. Clearly, the reliability of the model in describing the correct, say, kinetics of precipitation and morphology of precipitates will depend on the choice of the key parameters and on how acceptable the use of simple laws - such as 9 or 11 - is, for the specific physical system to be studied.

6.2 Results

In Fe-Cr alloys there are two experimentally observed phenomena that can be studied using a vacancy jump AKMC algorithm and therefore used as a test for the proposed interatomic potentials: the nanosegregation of α' phase and the inverse Kirkendall effect. The nanosegregation, or precipitation, of α' phase, not only under irradiation [8], but also during thermal treatments, is a well and long known phenomenon (475°C embrittlement, see e.g. [31]), with a clear impact on the mechanical properties of Fe-Cr ferritic alloys. The inverse Kirkendall effect is used to explain why depletion of Cr atoms takes place under irradiation close to vacancy sinks (e.g. at grain boundaries). The latter process is typical of austenitic steels, but has also been reported in ferritic steels and it is in a ferritic matrix that it has been simulated.

6.2.1 Phase separation

To check whether the interatomic potentials can predict α' Cr-rich phase separation at higher Cr concentrations, a thermal ageing process was reproduced: in a cubic box with side equal to 60 lattice units (432000 atoms), the evolution of an Fe-15%Cr alloy thermally treated at 800 K was simulated, by introducing only one vacancy in the system. This corresponds to a vacancy concentration roughly 12000 times larger than the equilibrium vacancy concentration expected at 800 K in the alloy (assuming a vacancy formation energy of 1.54 eV, as predicted by the interatomic potentials used, and neglecting the small binding energy of the vacancy to Cr atoms, as well as the entropy of formation), but this difference is easily and customarily accounted for by simply rescaling the simulated time to a corresponding real time about 12000 times longer [94]. The 15%Cr concentration was chosen purposely in order to test the potentials outside their fitting range. While from figure 6 the FM-5 is not expected to reproduce phase separation, no definitive answer can be given for the other potentials without a test of this type. The simulation was protracted up to 2 billion vacancy jumps with FM-5 and FM-10, while with PM-10 and FM-20 it was prolonged up to 4 billion jumps, in order to simulate the same timespan (about 0.5 seconds, to be adequately rescaled to obtain the corre-

sponding real time). This factor 2 difference in the simulated time after 2 billion vacancy jumps is the result of the non linear dependence of the AKMC timestep duration on the activation energy for migration, which depends, in turn, in a complex way on the binding energies between vacancies and solute atoms predicted by the interatomic potential used. Two billion vacancy jumps required about 100 hours of CPU time on an Optiplex GX240, Pentium IV, 2GHz processor. The results are shown in figures 8 to 13. In figure 8 the total energy of the system is plotted versus time according to the four interatomic potentials.

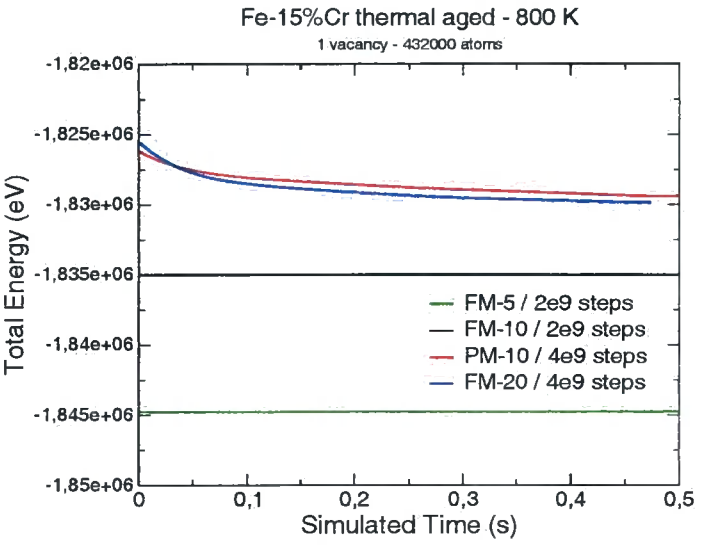

Fig. 8. Evolution in time of the total energy of the Fe-15%Cr systems, according to the four EAM potentials considered in this work. Only FM-20 and PM-10 predict phase separation.

The rapid decrease till steady state exhibited by PM-10 and FM-20 is typical of ongoing precipitation till the percentage of solute atoms in solution becomes smaller than the solubility limit predicted by the potential (respectively, 2.51% and 2.34% for PM-10 and FM-20 according to this simulation). On the contrary, FM-5 and FM-10 do not show any decrease in energy, meaning that the lowest energy state for these potentials is the random alloy.

This picture is confirmed by figures 9, 10 and 11, where the integral Cr-Cr pair correlation function corresponding to initial and final atomic configurations is represented at increasingly small scale. The curves correspond to the probability that a Cr-Cr pair is found at a distance less than the distance specified in abscissae (the sum of the points equals one). The fact that the PM-10 and FM-20 curves are shifted to the left for small distances means that the probability of finding close Cr-Cr pairs is higher than in the other case, i.e. precipitation has taken place. In figure 9 the initial curve is indis-

tinguishable from the final curves for FM-5 and FM-10, indicating that the alloys were random at the beginning and remain random at the end, while no large difference is visible between PM-10 and FM-20. Indeed, the differences between close curves are very small and become increasingly visible only by going to finer scales (figures 10 and above all 11). In the latter figure a slight tendency to further repulsion and further attraction is observed with, respectively, FM-5 and FM-10 (lower and higher probabilities of finding first nearest neighbour Cr atoms). In addition, it can be seen that PM-10 predicts a slightly reduced amount of precipitation as compared to FM-20. Finally, in figures 12 and 13 the initial and final atomic configurations in the FM-20 simulation are visualised and the formation of large precipitates is clearly visible. All these evidences reveal that the precipitates contain often only Cr atoms.

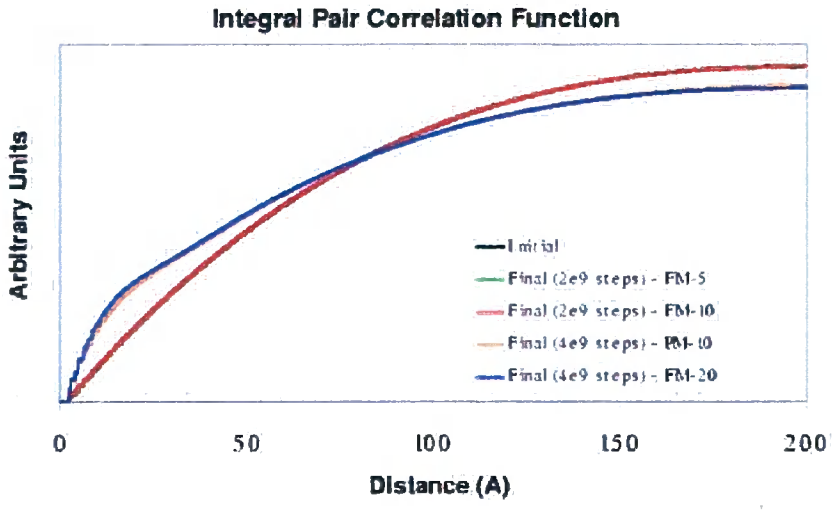

Fig. 9. Integral pair correlation function at the beginning and the end of the simulation using the four EAM interatomic potentials considered in this work. At this scale, no difference is visible between the beginning and the end when using FM-5 and FM-10 (random solution in both case), while no difference can be made out between PM-10 and FM-20, where phase separation takes place.

In conclusion, the fitting to high mixing enthalpies (PM-10, FM-20) does produce a different behaviour and allows the prediction of phase separation, which is not described by lower concentration potentials. However, the result of the simulation is that pure Cr is segregated, instead of Cr-rich α' phase containing about 80-85% Cr, so that, even assuming that different potentials should be

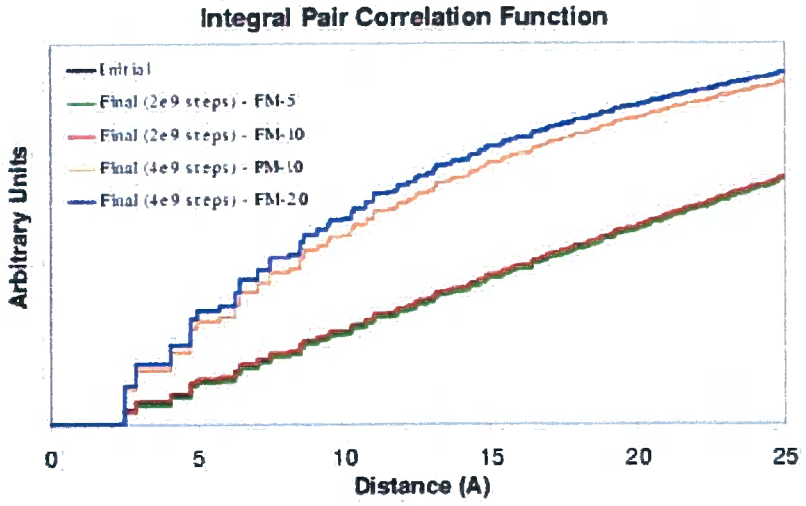

Fig. 10. Same as previous figure, at smaller scale. PM-10 segregatges less than FM-20.

fitted to work at different concentrations (*concentration dependent potentials*), in any case some work has still to be done in order to predict the correct type of phase separation.

6.2.2 Inverse Kirkendall effect

In an irradiated binary alloy A-B, if the partial diffusion coefficients D_A^V and D_B^V (where V specifies the vacancy migration mechanism) are different, the vacancy flux J_V to the sink will cause different atom fluxes J_A and J_B in the opposite direction. The faster diffusing species will indeed exchange more often position with the irradiation induced vacancies migrating to the sink, with the net result of a depletion of the faster transported constituent near the sink, and an enrichment of the slower one [95]. This phenomenon is typically used to explain the observed Cr depletion at grain boundaries in irradiated austenitic steels, which is regarded as a possible cause of loss of corrosion resistance (sensitisation) [96]. In ferritic steels Cr depletion at sinks is less evident and depends markedly on dose and temperature, but is conclusively known to take place [97].
To simulate the effect of the inverse Kirkendall effect in a ferritic matrix the following procedure was used. In a cubic box with side equal to 80 lattice units (1024000 atoms) a rigid lattice of Fe, alloyed with 3% randomly distributed

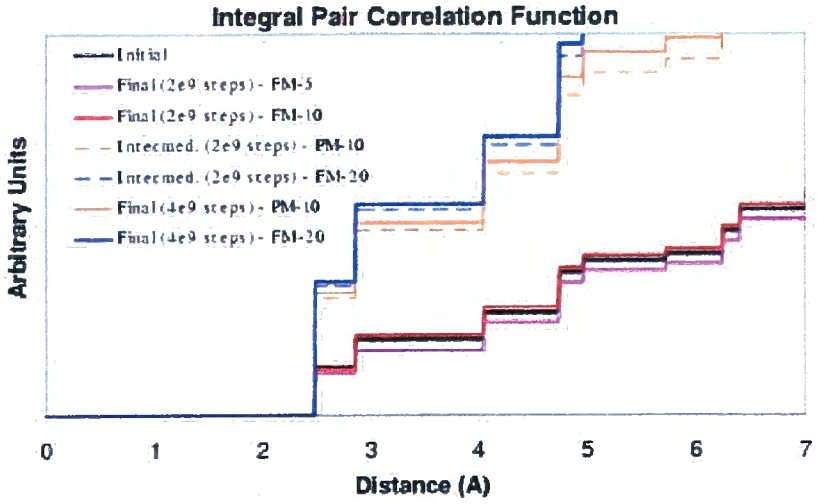

Fig. 11. Same as previous figure, at even smaller scale, including intermediate state for PM-10 and FM-20. FM-5 shows tendency to further separation between Cr atoms (ordering tendency).

Cr atoms, was built. At the centre of the box 50 vacancies were randomly distributed within a sphere of 3 nm radius, roughly simulating the effect of introducing a displacement cascade initiated by a recoil of about 20 keV, after disappearance of the SIA. This is of course far from reproducing the real effect of a displacement cascade, but it is a way of introducing a local supersaturation of vacancies, similar to a displacement cascade. The AKMC simulation was run at 800 K with absorbing boundary conditions (vacancies that reached the boundary disappeared for good from the simulation box), roughly simulating the grain boundary of a cubic nanocrystal. Again, this is far from reproducing the real effect of a grain boundary, but corresponds to introducing an extended sink in the simulation. The constant energy barrier E_0 was set to 0.68 eV for Fe atoms and 0.58 for Cr atoms, as calculated using VASP (see table 6). The simulation was run until all the vacancies initially introduced in the box disappeared through the boundaries. At that point, the simulation was restarted by introducing a new pseudo-cascade, and so on. This was repeated 1000 times and the rate of disappearance of the vacancies turned out to be rather regular. It can be said that about 0.05 dpa were accumulated in the simulation volume, with an overall resulting dose rate of about $6 \cdot 10^{-2}$ dpa s^{-1}.

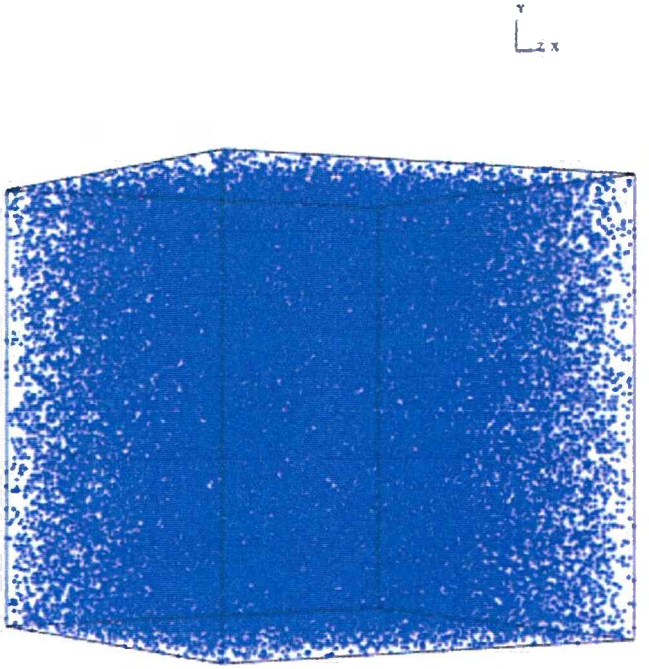

Fig. 12. Initial distribution of Cr atoms.

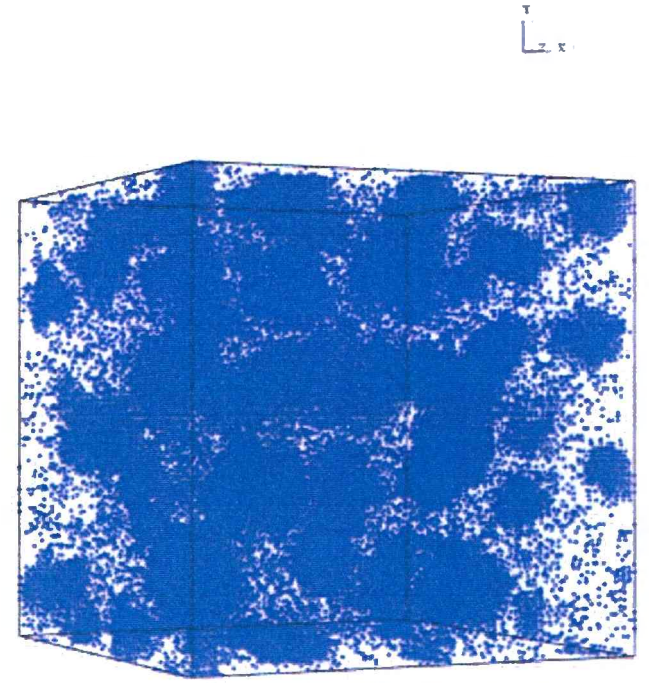

Fig. 13. Final distribution of Cr atoms using FM-20 (biggest precipitation effect).

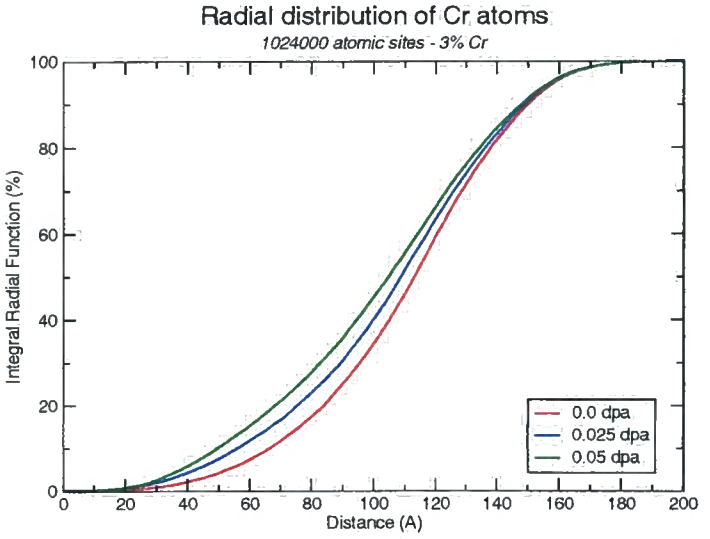

Fig. 14. The inverse Kirkendall Effect

The simulation took about 2 months of CPU time to be completed on an Optiplex GX240, Pentium IV, 2GHz processor. In figure 14 the result obtained using the FM-10 potential is shown. The integral radial distribution function of Cr atoms measured from the centre of the box is shown at the beginning and after accumulating 0.025 and 0.05 dpa. The meaning of this function is the probability that a Cr atom is encountered at a distance less than the distance in abscissae. The fact that the curve is clearly seen to shift to the left with increasing dose means that while dose is accumulated Cr atoms are moving inwards. Therefore, this simple model is actually sensitive to the lower migration energy assigned to Cr and low binding energy between Cr atoms and vacancies predicted by the interatomic potential: vacancies are not trapped at solute atoms and effectively migrate towards the sink and the inverse Kirkendall effect for Cr atoms is nicely reproduced.
The extremely long CPU time required by this type of simulation advised against repeating the process with all four potentials. However, according to the study presented in this report FM-5 is expected to behave in much the same way as FM-10, while FM-20 and PM-10 are known to provide very similar predictions. An attempt was therefore made with FM-20, which was soon interrupted because very quickly a large void was formed at the centre of the simulation box (about 400 vacancies after a few tens of repetitions). This unphysical result should most likely be attributed to too high V-V and V-Cr unrelaxed binding energies predicted by FM-20, to be confirmed by a calculation of the dependence of these energies on Cr concentration. Indeed, vacancy trapping at Cr atoms and high V-V binding energies are the two obvious ingredients for rapid nucleation and growth of voids. Needless to say, looking for an inverse Kirkendall effect in this situation would be a hopeless search.

Of course, the unphysical result may also be the consequence of inadequacies of the simplistic model used. However, this result does act as a caveat against possible undesired backlashes of some fitting parameters.

7 Discussion and conclusions

In this report four recently fitted long-range Embedded Atom Method potentials for Fe-Cr alloys and, to a lesser extent, also a short-range Finnis-Sinclair potential for the same alloy, have been tested by calculating basic alloy properties of interest for radiation damage studies (lattice parameter and mixing enthalpy versus Cr concentration, energies of formation and interaction of Cr atoms with themselves and point defects, migration energies) and comparing the result with available *ab initio* values and experimental evidence, as well as with an older Fe-Cr potential by Farkas and co-workers. The difference between the four EAM potentials is determined by the mixing enthalpy and bulk modulus values used for the fitting, which correspond to increasing Cr concentrations or different magnetic properties of the same alloy. The EAM potentials were also tested on Atomistic Kinetic Monte Carlo simulations based on the vacancy jump algorithm, to check at least qualitatively their capability of predicting Cr-rich α' phase separation.
Ideally, based on the *ab initio* data and experimental evidence discussed in this report, an interatomic potential for Fe-Cr should have the following features:
1- It should describe as reliably as possible pure Fe and pure Cr; in particular, it should yield the *right* SIA configuration in Fe and the negative Cauchy pressure in Cr, which are the two *problematic* issues in these metals respectively, but also give an acceptable description of vacancies, especially from the point of view of the binding energies, which determine the stability of voids.
2- It should predict negligible interaction between Cr and vacancies and the stability of the mixed dumbbell, with a reasonably strong attractive interaction between SIA and Cr atoms.
3- It should predict as correctly as possible the change of sign of the mixing enthalpy as a function of Cr concentration (negative below about 6% Cr, positive above) and therefore the region of α-α' phase co-existence allowed for by the Fe-Cr phase diagram.
About point 1, none of the potentials is completely satisfactory. This is not surprising because these are the known limitations of the EAM and FS approaches. It has been long shown that no simple EAM or FS potential can properly describe the elastic properties of Cr, while the problem of the *right* interstitial is related to the apparent incompatibility, also stemming from the adopted formalisms, between long-range choice and prediction of the $\langle 110 \rangle$ interstitial. Nonetheless, these approaches have the advantage of being simple and portable and these advantages have hitherto outweighed their *minor*

shortcomings. All the more in the light of the fact that no modified EAM method has so far proven to be definitively superior, since all the modified approaches proposed in the literature were introduced to solve limited problems (e.g. the negative Cauchy pressure in Cr), without giving any global appraisal of the general performance of the particular proposed alternative, compared to original EAM or FS. In addition, the work currently in progress seems to show that minor adjustments may finally overcome the problems encountered using the EAM approach to describe Fe and Cr.

About point 2, the FM-5 and FM-10 potentials seem to meet the requirement rather well, in fact better than any existing potential for Fe-Cr systems. The difference between them is only given by the fact that FM-5 predicts repulsion between Cr atoms, as it has been fitted to a negative mixing enthalpy, and therefore should be used in the range of negative mixing enthalpy, while the other is more adequate for the region of positive mixing enthalpy, at least below the concentration where phase separation becomes definitively visible and starts to have an important role in radiation effects. At any rate, phase separation is not really expected to be an in-cascade phenomenon, so that for the purpose of simulating displacement cascades at a Cr concentration around 10% FM-10 is possibly the best choice currently available.

The phase separation issue leads us to consider point 3. The potential labelled as FM-20 was fitted for the purpose of describing the regions of Cr concentration where phase separation takes place in ferromagnetic alloys. As a matter of fact, it does predict phase separation, but the segregated phase does not seem to be the α' phase, as desired, at least according to KMC simulations on rigid lattice. In reality, only more time demanding calculations (such as Metropolis Monte Carlo with relaxation) could give a definitive answer about the actual capability of these potentials, as far as phase separation is concerned. However, there are strong suspects that, by fitting the potential to a high mixing enthalpy value, undesired side effects may appear, such as the loss of the interaction with SIA and the increase in the V-Cr binding energy. The reason for this can be that the potential predicts the right mixing enthalpy only at the concentration for which it was fitted: the *real* (at least according to *ab initio* calculations) shape of the curve is not reproduced at all, by any potential, not even locally.

A possible solution to this problem is the fabrication of a *concentration dependent* potential. This dependence would not be embodied by an additional term in the mathematical form of the potential, but by the production of a series of tabulated potentials, among which the *right* one has to be chosen each time by the MD code, according to an *on-the-fly* evaluation of the local concentration. In principle, the implementation of this approach should not increase the computing time in an unacceptable way and may indeed be a simple, if *brute force*, solution. There are, however, a series of possible problems. First of all, the volume used for the determination of the local concentration around an atom will always be somewhat arbitrary and sensitivity studies should be conducted to find the optimal choice, compromise between accuracy, stability

of the results and computing time. Secondly, if the concentration at equilibrium is an obvious magnitude, it may not be so in the presence of defects. Finally, the choice of the number of potentials to be fitted is also arbitrary and because none of them seems to be able to reproduce the shape of the mixing enthalpy curve, it is as if a discontinuous mixing enthalpy curve was used, with a grain of discontinuity arbitrarily small. All these aspects would most likely add uncertainties to the model.
Another possible solution could be to try to fit the potential in such a way that the whole mixing enthalpy curve is reproduced. This is clearly not achievable with only one mixing enthalpy fitting parameter, but may be possible with two, such as the slope of the curve at 0% Cr (the heat of solution, equal to the substitution energy of a Cr atom in Fe) and the node, i.e. the zero of the mixing enthalpy for a non vanishing Cr concentration. This, however, may oblige to give up other fitting parameters, such as the lattice parameter or the cohesive energy for the alloy, or, alternatively, to increase the number of free parameters in the mathematical form of the potential. However, even this route may not lead to the desired solution.
There is also another *caveat* to be taken into account. The PM-10 potential, which reproduces rather well the curve of the mixing enthalpy for the paramagnetic alloy, still gives predictions very similar to FM-20, as far as phase separation is concerned, so that the suspect arises that the mixing enthalpy fitting may not be sufficient to predict the right phase separation. On the other hand, according to the phase diagram no phase separation occurs in the range of temperature where the system is paramagnetic.

In conclusion, it can be said that the potential labelled as FM-10 seems to be at the moment the best available choice to simulate displacement cascades in Fe-Cr alloys in the range of low Cr concentrations where phase separation is not an issue and the mixing enthalpy of the system is positive. The main shortcoming of this potential is the prediction of the most stable interstitial configuration in Fe, which is however probably outweighed by its long-range nature and the acceptable description of Cr/point-defect interactions. In addition, this problem may be overcome in the near future. The issue of describing phase separation is a more complex one, for which no definitive answer can be given at the moment. Possible routes towards the solution of this problem are the fabrication of a set of concentration dependent potentials or different fitting strategies.

8 Acknowledgements

P.O. would like to thank the staff of LHMA at SCK-CEN in Mol, Belgium, for the very nice period of time he spent there. He would also like to thank the people in the dormitories for being good friends and the two volleyball teams:

BR1 and Nuclea 2 for a good time. The authors are indebted, for their fundamental contribution to this report, to: C. Domain (EDF), who provided the VASP data; F. Chami (University of Sheffield), who performed *ad hoc* calculations with Konishi's potential that highly enriched this report; R. Chakarova and V. Pontikis, who produced two of the four EAM interatomic potentials; and J. Wallenius who, together with the authors, has been the driving force for the establishment and conduction of the collaboration between Belgium and Sweden on the Fe-Cr issue. The authors would also like to thank J. Kallne and M. Décreton for making P.O.'s stay in Mol a reality, as well as STINT, Sweden, and the EC fusion programme for financial support, under the Agreement for the Promotion of Staff Mobility No. 131-83-7 FUSC.

References

[1] R. L. Klueh, K. Ehrlich and F. Abe, *Ferritic/martensitic steels: promises and problems*, J. Nucl. Mater. 191-194 (1992) 116-124.

[2] T. Auger, L. Aphecetche, A. Cadiou, Y. Dai, H. Glasbrenner, F. Gröschel and T. Kirchner, *MEGAPIE target design and LiSoR experiment - Status report*, J. Phys. IV France 12 (2002) 8-27.

[3] A.-A.F. Tavassoli, *Present limits and improvements of structural materials for fusion reactors*, J. Nucl. Mater. 302 (2002) 73-88.

[4] C. Cawthorne and E. J. Fulton, *Voids in irradiated stainless steel*, Nature 216 (1967) 575-576.

[5] F. A. Garner, M. B. Toloczko and B. H. Sencer, *Comparison of swelling and irradiation creep behaviour of fcc-austenitic and bcc- ferritic/martensitic alloys at high neutron exposure*, J. Nucl. Mater. 276 (2000) 123-142.

[6] A. Kohyama, A. Hishinuma, D. S. Gelles, R. L. Klueh, W. Dietz and K. Ehrlich, *Low-activation ferritic and martensitic steels for fusion applications*, J. Nucl. Mater. 233-237 (1996) 138-147.

[7] R. L. Klueh and D. J. Alexander, *Effect of heat treatment and irradiation temperature on impact properties of Cr-W-V ferritic steels*, J. Nucl. Mater. 265 (1999) 262-272.

[8] M. H. Mathon, Y. de Carlan, G. Geoffroy, X. Averty, A. Alamo and C. H. de Novion, *A SANS investigation of the irradiation-enhanced α-α' phases separation in 7-12 Cr martensitic steels*, J. Nucl. Mater. 312 (2003) 236-248.

[9] V. V. Rybin, I. P. Kursevich and A. N. Lapin, *Effect of neutron irradiation at low temperature on the embrittlement of the reduced-activation ferritic steels*, J. Nucl. Mater. 258-263 (1998) 1324-1328.

[10] R. L. Klueh, D. J. Alexander and M. A. Sokolov, *Effect of chromium, tungsten, tantalum and boron on mechanical properties of 5-9Cr-WVTaB steels*, J. Nucl. Mater. 304 (2002) 139-152.

[11] C. H. Woo and B. N. Singh, *Production bias due to clustering of point defects in irradiation-induced cascades*, Phil. Mag. A 65 (1992) 889- 912.

[12] B. N. Singh, S. I. Golubov, H. Trinkaus, A. Serra, Yu. N. Osetsky and A. V. Barashev, *Aspects of microstructure evolution under cascade damage conditions*, J. Nucl. Mat 251 (1997) 107-122.

[13] S. I. Golubov, B. N. Singh and H. Trinkaus, *Defect accumulation in fcc and bcc metals and alloys under cascade damage conditions– Towards a generalisation of the production bias model*, J. Nucl. Mat. 276 (2000) 78-89.

[14] B. N. Singh and J. H. Evans, *Significant differences in defect accumulation between fcc and bcc crystals under cascade damage conditions*, J. Nucl. Mat. 226 (1995) 277-285.

[15] A. F. Calder and D. J. Bacon, *A molecular dynamics study of displacement cascades in α-iron*, J. Nucl. Mat. 207 (1993) 25-45.

[16] R. E. Stoller, *The role of cascade energy and temperature in primary defect formation in iron*, J. Nucl. Mat. 276 (2000) 22- 32.

[17] W. J. Phytian, R. E. Stoller, A. F. Calder, A. J. E. Foreman and D. J. Bacon, *A comparison of displacement cascades in copper and iron by molecular dynamics and its application to microstructural evolution*, J. Nucl. Mater. 223 (1995) 245.

[18] M. Daw and M. Baskes, Phys. Rev. B 29 (1984) 6443 .

[19] M. W. Finnis, J. E. Sinclair, *A simple empirical N-body potential for transition metals*, Phil. Mag. A 50 (1984) 45-55.

[20] F. Gao, D. J. Bacon, Yu. N. Osetsky, P. E. J. Flewitt and T. A. Lewis, *Properties and evolution of sessile interstitial clusters produced by displacement cascades in α-iron*, J. Nucl. Mater. 276 (2000) 213-220.

[21] G. Simonelli, R. Pasianot and E. J. Savino, *Embedded-atom-method interatomic potentials for bcc-iron*, Mat. Res. Soc. Symp. Proc. 291 (1993).

[22] C. S. Becquart, C. Domain, A. Legris, J-C. van Duysen, *Influence of the interatomic potentials on molecular dynamics simulations of displacement cascades*, J. Nucl. Mat. 280 (2000) 73-85.

[23] J. F. Ziegler, J. P. Biersack, U. Littmark, *The stopping and range of ions in solids*, Vol.1, Ed. J.F. Ziegler, Pergamon, New York (1985).

[24] L. Malerba, unpublished results.

[25] E. A. Little, D. A. Stow, *Void-swelling in iron and ferritic steels. II. An experimental survey of materials irradiated in a fast reactor*, J. Nucl. Mat. 87 (1979) 25.

[26] S. I. Porollo, A. M. Dvoriashin, A. N. Vorobyev and Yu. V. Konobeev, *The microstructure and tensile properties of Fe-Cr alloys after neutron irradiation at 400° C to 5.5-7.1 dpa*, J. Nucl. Mat. 256 (1998) 247-253.

[27] A. Okada, H. Maeda, K. Hamada and I. Ishida, *Defect structure development in a pure iron and dilute iron alloys irradiated with neutrons and electrons*, J. Nucl. Mater. 271&272 (1999) 133-138.

[28] N. Yoshida, A. Yamaguchi, T. Muroga, Y. Miyamoto and K. Kitajima, *Characteristics of point defects and their clustering in pure ferritic steels*, J. Nucl. Mater. 155-157 (1988) 1232-1236.

[29] F. Maury, P. Lucasson, A. Lucasson, F. Faodo and J. Bigot, *A study of irradiated FeCr alloys: deviations from Matthiessen's ruel and interstitial migration*, J. Phys: Metal Phys. 17 (1987) 1143.

[30] H. Kuwano and Y. Hamaguchi, *Mössbauer study of iron-chromium alloys irradiated by energetic protons*, J. Nucl. Mat. 155-157(1988) 1071-1074.

[31] R. Lagneborg, *Metallography of the 475° C embrittlement in an iron-30% chromium alloy*, Transaction of the ASM 60 (1967) 67-78.

[32] P. Olsson, I. A. Abrikosov, L. Vitos and J. Wallenius, *Ab initio formation energies of Fe-Cr alloys*, in print: J. Nucl. Mater.

[33] C. Domain and C.S. Bequart, *Ab initio calculations of defects in Fe and dilute Fe-Cu alloys*, Phys. Rev. B 65 (2002) 024103.

[34] C.S. Bequart, C. Domain, *Ab initio contribution to the study of complexes formed during dilute Fe-Cu alloys radiation*, Nucl. Instr. & Meth. B 202 (2003) 44-50.

[35] M. P. Allen and D. J. Tildesley *Computer Simulation of Liquids*, Clarendon Press, Oxford (1987).

[36] P. Olsson, R. Chakarova, J. Wallenius and V. Pontikis, *Modelling of radiation damage in Fe-Cr alloys*, submitted to Phys. Rev. B (2003); R. Chakarova, V. Pontikis and J. Wallenius, *Development of FeCr many body potential and cohesion model*, Delivery Report WP6 - SPIRE project, contract no. FIKW-CT-2000-00058 (June 2002).

[37] T. Konishi, K. Ohsawa, H. Abe and E. Kuramoto, *Determination of N-body potential for Fe-Cr alloy system and its application to defect study*, Comput. MAter. Sci. 14 (1999) 108-113.

[38] R. Bullough and M. H. Wood, *Theory of Microstructural Evolution*, in: *Physics of Radiation Effects*, Eds. R. A. Johnson and A. N. Orlov, North Holland Physics Publishing, Elsevier Science Publishers B. V. (1986) 189-224.

[39] A. Hardouin Duparc, C. Moingeon, N. Smetniansky-de-Grande and A. Barbu, *Microstructure modelling of ferritic alloys under high flux 1 MeV electron irradiations*, J. Nucl. Mater. 302 (2002) 143-155.

[40] F. Soisson, A. Barbu and G. Martin, *Monte Carlo Simulations of Copper Precipitation in Dilute Iron-Copper Alloys during Thermal Ageing and Under Electron Irradiation*, Acta Mater. 44(9) (1996) 3789-3800.

[41] B. D. Wirth, G. R. Odette, D. Maroudas and G. E. Lucas, J. Nucl. Mater. 244 (1997) 185.

[42] C. Domain, C. S. Becquart and J-C. van Duysen *Kinetic Monte Carlo simulations of FeCu alloys*, Mater. Res. Soc. Symp. Proc. 540 (1999) 643-648.

[43] H. L. Heinisch and B. N. Singh, *Stochastic annealing simulation of intracascade defect interactions*, J. Nucl. Mater. 251 (1997) 77-85.

[44] N. Soneda and T. Diaz de la Rubia, *Defect production, annealing kinetics and damage evolution in α-Fe: an atomic-scale computer simulation*, Phil. Mag. A 78 (1998) 995-1019.

[45] E. Alonso, M. J. Caturla, T. Diaz de la Rubia, N. Soneda, J. Marian, J. M. Perlado and R. E. Stoller, *Comparative study of damage accumulation in iron under magnetic and inertial fusion conditions*, J. Nucl. Mater. 283-287 (2000) 768-772.

[46] C. Domain, C. S. Becquart and J-C. van Duysen, *Kinetic Monte Carlo simulations of cascades in Fe alloys*, Mater. Res. Soc. Symp. Proc. 650 (2001) R3.25.1-6.

[47] C. Domain, C. S. Becquart and L. Malerba, *Simulation of radiation damage in Fe alloys: a kinetic Monte Carlo approach*, submitted to J. Nucl. Mater. (2003).

[48] O. K. Andersen, O. Jespen and G. Krier, *Lectures on Methods of Electronic Structure Calculations*, edited by V. Kumar, O. K. Andersen and A. Mookerjee, (World Scientific Publishing, Singapore, 1994) 63-124.

[49] O. K. Andersen, C. Arcangeli, R. W. Tank, T. Saha-Dasgupta, G. Krier, O. Jespen and I. Dasgupta, *Tight-binding Approach to Computational Materials Science*, edited by P. E. A. Turchi, A. Gonis and L. Colombo, MRS. Symp. Proc. 491 (Materials Research Society, Pittsburgh, 1998) 3-34.

[50] O. K. Andersen and T. Saha-Dasgupta, Phys. Rev. B 62 (2000) R16219.

[51] D. M. Ceperly and B. J. Alder, Phys. Rev. B 45 (1980) 566.

[52] I. A. Abrikosov and H. L. Skriver, Phys. Rev. B 47, (1993) 16532.

[53] L. Vitos, I. A. Abrikosov and B. Johansson, Phys. Rev. Lett 87 (2001)156401.

[54] I. A. Abrikosov and B. Johansson, Phys. Rev. B 57 (1998) 14164.

[55] I. Mirebeau, M. Hennion and G. Parette, Phys. Rev. Lett. 53 (1984) 687.

[56] C. Domain, unpublished results (2002).

[57] G. Kresse and J. Hafner, Phys. Rev. B 47 (1993) 558.

[58] G. Kresse and J. Hafner, Phys. Rev. B 49 (1994) 14251.

[59] G. Kresse and J. Furthmller, Comput. Mat. Sci. 6 (1996) 15.

[60] W.A. Dench, Trans. Faraday Soc. 59 (1962) 1279-1292.

[61] R. Hultgren et. al., *Selected Values of Thermodynamic Properties of Binary Alloys*, (Ohio 1973) 694-703.

[62] D. Farkas, C. G. Schon, M. S. F. De Lima and H. Goldenstein, *Embedded atom computer simulation of lattice distortion and dislocation core structure and mobility in Fe-Cr alloys*, Acta Mater. 44 (1996) 409-419.

[63] F. Chami, C.M. Care and R. Smith, *Molecular dynamics simulation of bulk and surface damage production in α-Fe by Cr bombardment*, to be submitted to Rad. eff. & Def. in Solids.

[64] F. Chami, unpublished results (2003).

[65] A version in C is available at the following website: http://www.ims.uconn.edu/centers/simul/index.htm\Rifkin#xmd.

[66] B. J. Alder, T. E. Wainwright, J. Chem. Phys. 27 (1957) 1208.

[67] B. J. Alder, T. E. Wainwright, J. Chem. Phys. 31 (1959) 459.

[68] B. J. Alder, T. E. Wainwright, J. Chem. Phys. 33 (1960) 1439.

[69] J. B. Gibson, A. N. Goland, M. Milgram and G. H. Vineyard *Dynamics of Radiation Damage*, Phys. Rev. 120(4) (1960) 1229-1253.

[70] J. B. Adams, A. Rockett, J. Kieffer, W. Xu, M. Nomura, K. A. Kilian, D. F. Richards and R. Ramprasand, J. Nucl. Mater. 216 (1994) 265.

[71] W.B. Pearson, *A handbook of lattice spacings and structures of metals and alloys*, (Belfast 1958) 532-533.

[72] G.J. Ackland, D.J. Bacon, A.F. Calder and T. Harry, Phil. Mag. A 75 (1997) 713-732.

[73] H. Schultz and P. Ehrhart, in Atomic Defects in Metals, edited by H. Ullmaier, Landolt-Börnstein, New Series, Group III, Vol. 25 (Springer, Berlin, 1991), p. 115

[74] H.E. Schaefer, K. Maier, M. Weller, D. Herlach, A. Seeger and J Diehl, Scripta metall 11 (1977) 803.

[75] K. Frderer, K.P. Döring, M. Gladisch, N. Haas, D. Herlach, J. Major, H.J. Mundinger, J. Rozenkrantz, W. Schaefer, L. Schimmele, M. Schmolz, W Schwarz and A. Seeger, Mater. Sci. Forum 15-18 (1987) 125.

[76] P. Ehrhart, H.D. Carstanjen, A.M. Fattah and J.B. Roberto, Phil. Mag. A 40 (1979) 843.

[77] L. De Schepper, G. Knuyt, L.M. Stals, D. Segers, L. Dorikens-Vanpraet, M. Dorikens and P. Moser, Mater. Sci. Forum 15-18 (1987) 131.

[78] K. Masuda, *Calculation of interaction energy between atomic defects in bcc transition metals: Vacancy-vacancy, vacancy-vacancy cluster and vacancy-impiruty pairs*, in: *Point Defects and Defect Interactions in Metals*, J. Takamura, M. Doyama and M. Kiritani Eds., U. of Tokyo press (1982)105-107; J. Phys. (France) 43 (1982) 921.

[79] A. Weidinger, R. Wessner, T. Wichert and E. Recknagel, Phys. Lett. 72A (1979) 369.

[80] C. Demangeat *Impurity-vacancy and vacancy-vacancy binding energies in α-iron*, Phil. Mag. 32(1) (1975) 323-331.

[81] E. Kuramoto, S. Nagano, K. Nishi, K. Makii, Y. Aono and M. Takenaka, *Positron aniihilation lifetime measurements of electron irradiated FeCr alloys*, Mater. Sci. Forum 105-110 (1992) 1125.

[82] A. Wolfe, H.W. Paxton, *Diffusion in bcc metals*, Trans. Metallurgical Soc. AIME 230 (1964) 1426.

[83] A. Möslang, E. Albert, E. Recknagel and A. Weidinger, *Interaction of vacancies with impurities in Fe*, Hyperfine Interactions 15/16 (1983) 409-412.

[84] V. Hivert, R. Pichon, H. Bilger, P. Bichon, J. Verdone, D. Dautreppe and P. Moser, J. Phys. Chem. Solids 31 (1970) 1843.

[85] P. Ehrhart, J. Nucl. Mater. 69-70 (1978) 200.

[86] P. Ehrhart, K. H. Robrock and H. R. Schober in: Physics of Radiation effects in Crystals, edited by R. A. Johnson and A. N. Orlov (Elsevier, Amsterdam, 1986), 63.

[87] H. Abe, S. Takamura, N. Yoshida and K. Kitajima, Bull. Res. Inst. Appl. Mech. 63 (1987) 143.

[88] W. Schilling *Self-interstitial atoms in metals*, J. Nucl. Mater. 69&70 (1978) 465-489.

[89] F. Gao, G. Henkelman, W. J. Weber, L. Rene Corrales and H. Jonsson, Nucl. Instr. Meth. B 202 (2003) 1-7.

[90] A. D. Le Claire, *Solvent self-diffusion in dilute BCC solid solutions*, Phil. Mag. 172 (1970) 819-832.

[91] D. Terentyev and L. Malerba, work in progress.

[92] F. S. Buffington, K. Hirano and M. Cohen, Acta Met. 9 (1961) 434.

[93] W. M. Young and E. W. Elcock, *Monte Carlo studies of vacancy migration in binary ordered alloys: I*, Proc. Phys. Soc. 89 (1966) 735-746.

[94] S. Schmauder and P. Binkele, *Atomistic computer simulation of the formation of Cu-precipitates in steels*, Comput. Mater. Sci. 24(1-2) (2002) 42-53.

[95] H. J. Wollenberger *Point Defects* in: *Physical Metallurgy*, R. W. Cahn and P. Haasen Editors, Elsevier Science (1996) 1621 (chapter 18).

[96] T. R. Allen, J. T. Busby, G. S. Was and E. A. Kenik *On the mechanisms of radiation induced segregation in austenitic Fe-Cr-Ni alloys*, J. Nucl. Mater. 255(1) (1998) 44-58.

[97] E. A. Little, J. Nucl. Mater. 206 (1993) 324.